2,5-Diiodothiophene: A Versatile Halogen Bonding Synthon for Crystal Engineering

Arianna C. Ragusa[†], Andrew J. Peloquin[†], Colin D. McMillen[†,], and William T. Pennington[†,*]*

[†]Department of Chemistry, Clemson University, 219 Hunter Laboratories, Clemson, SC 29634-0973, USA. cmcmill@clemson.edu. billp@clemson.edu.

Abstract

Relative to the common diiodobenzene-based halogen bond donors, little is known about the halogen bonding of iodine-substituted thiophene compounds. A series of cocrystallization experiments were performed using the sulfur atom-containing halogen bond donor 2,5-diiodothiophene with *N*-heterocyclic diamines as well as ammonium iodide salts. These results reveal a wide range of halogen bonding motifs tied to the halogen bond donor/acceptor stoichiometry. While in acceptor rich stoichiometries discrete units prevail through C–I···I halogen bonds, donor rich stoichiometries encourage the formation of 2-dimensional halogen bonding networks, often with the additional involvement C–I···S and S···S interactions. Halogen bonding through the C–I iodine atom predominates in all structures. The measured halogen bond distances fall between those typically observed for 1,4-diiodobenzene and 1,4-diiodotetrafluorobenzene, reaffirming the role of fluorination in strengthening the halogen bond while also expanding the library of halogen bonding synthons to donors having intermediate electrostatic potentials.

Introduction

Halogen bonding and the related chalcogen bonding interactions occur due to the anisotropic distribution of electron density on halogen or chalcogen atoms, resulting in attractive interactions between an electrophilic region on these atoms within a molecule and a nucleophilic region on a different atom or molecule.[1–4] This electrophilic region, referred to as the σ hole, is enhanced by the presence of electron-withdrawing substituents, such as in the diiodotetrafluorobenzene systems commonly used as halogen bond donors.[5–7]

With organoiodine halogen bond donors, most of the research has focused on nitrogen and oxygen as acceptor atoms, with sulfur typically receiving much less attention. While much of this attention is due to the prevalence of interactions with nitrogen and oxygen atoms in biological contexts,[8] sulfur is gaining attention as a potential halogen bonding-based drug design target.[9,10] For comparison, a survey of the Cambridge Structural Database (CSD),[11] limited to organics, yields 1576 and 2379 hits for C–I···N and C–I···O halogen bonds respectively, whereas a similar search for C–I···S halogen bonds yields only 407 results. Examples of structures with cooperative C–I···I and C–I···S interactions are even less common, with only 61 structures deposited in which both interactions are present.

Many of the notable examples of these structures containing both C–I···I and C–I···S interactions involve iodine-substituted tetrathiafulvalenes or dithianes. These molecules are often studied for their charge-transfer properties.[12–14] For example, the crystalline structure of 4,5-diiodo[1,2,5]thiadiazolotetrathiafulvalene displays S···N, S···S, S···I, N···I, and I···I interactions.[15] The structure of tetraiodotetrathiafulvalene reveals both C–I···I (3.8524(11) Å) and C–I···S (3.541(3) Å) halogen bonds.

Our group has also been interested in the structural tendencies of I···I and I···S halogen and chalcogen bonding as a crystal engineering tool.[16–20] The study of new synthons, such as thiophenes, presents an exciting extension of these crystal engineering studies, as they can potentially be involved in both halogen and chalcogen bonding interactions. Thiophene-based materials have attracted attention for their potential use in thin films for polymeric solar cells.[21–24] While the crystal structure of 3,4-diiodo-2,5-dimethylthiophene, which itself requires synthesis from 2,5-dimethylthiophene under strongly acidic conditions, was reported in 2007 and the structure of 3,4,5-triiodo-2-methylthiophene was reported in 2019,[25,26] the crystal structure of 2,5-diiodothiophene was surprisingly not published until 2017.[27] No reports of cocrystals involving halogen or chalcogen bonding have been reported with this simple substrate, nor has 2,5-diiodothiophene (**25DIT**) been reported in any other cocrystal composition. Being inexpensive and readily available from commercial sources, this substrate represents an ideal candidate for the study of the cooperation of C–I···I and C–I···S interactions when both can be operable. Herein we report 19 cocrystals involving 2,5-diiodothiophene as a halogen bond donor. Through systematic variation of halogen bond acceptor, utilizing ditopic amines, numerous iodide or triiodide salts, and donor:acceptor stoichiometry, a rich assortment of halogen and chalcogen bonding motifs were observed.

Experimental

Synthesis of cocrystals

Co-crystals were obtained using commercially available reagents, which were used as received. Reagents were dissolved in a minimum amount of methanol, ethanol, or acetonitrile. The solutions were allowed to evaporate slowly at room temperature. Vials were sealed to halt

evaporation as soon as crystals were observed to ensure sample purity. See ESI for full, specific crystal synthesis details.

X-ray structure determination

Crystals were mounted on low background cryogenic loops using paratone oil for single-crystal X-ray analysis. Data were collected using Mo Kα radiation (λ = 0.71073 Å) on a Bruker D8 Venture diffractometer with an Incoatec Iμs microfocus source and a Photon 2 detector. Diffraction data were collected using ϕ and ω-scans and subsequently processed and scaled using the APEX3 software suite (SAINT/SADABS).[28] The structures were solved with the SHELXT structure solution program and refined utilizing SHELXL, both incorporated in the *OLEX2* (v1.3) program package.[29–31] All nonhydrogen atoms were refined anisotropically. Using the appropriate riding models, all hydrogen atoms were placed in geometrically optimized positions. All geometric parameters within the manuscript body were calculated using *OLEX2*. Selected crystallographic and data collection parameters are listed in Table SI1. Additional details on the structural refinements, including the treatment of any disorder, are provided in the ESI.

Quantum theoretical calculations

All calculations were conducted using the Gaussian 09 Rev B.01 package with the *ω*B897X-D functional and the def2-TZVP basis set.[32–34] Molecular electrostatic potential calculations were performed on optimized geometries, and the surface potentials were extracted using MultiWFN version 3.7 with an isodensity value of 0.001 a.u.[35]

Results and Discussion

System design

As a halogen bond donor, 2,5-diiodothiophene is best compared with common linear halogen bond donors such as 1,4-diiodobenzene (**I2Bz**), 1,4-diiodotetrafluorobenzene (**I2F4Bz**), and 4,4'-diiodooctafluorobiphenyl (**I2F8bph**). The five-atom core of **25DIT** results in an I–C···C–I angle of 151.2(1)°C in the crystalline structure of pure **25DIT**, which varies little throughout this study. Lacking the fluorination of many other common halogen bond donors, the maximum electrostatic potential of **25DIT** is intermediate (28.0 kcal/mol) to **I2Bz** (22.7 kcal/mol) and **I2F4Bz** (32.6 kcal/mol) (Figure 1). These factors combine to make **25DIT** a suitable target of investigation as a new halogen bonding synthon for tuning the geometries and strength of halogen bonds in crystal engineering.

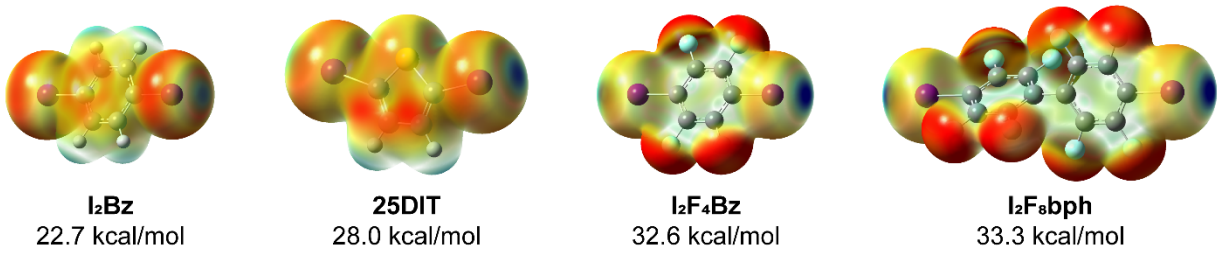

Figure 1. Electrostatic potential map of 2,5-diiodothiophene (**25DIT**), along with the other common halogen bond donors 1,4-diiodobenzene (**I_2Bz**), 1,4-diiodotetrafluorobenzene (**I_2F_4Bz**), and 4,4'-diiodooctafluorobiphenyl (**I_2F_8bph**). The electrostatic potential is calculated at the 0.005 au isodensity surface and ranges from -25 kcal/mol (red) to 38 kcal/mol (blue).

Cocrystals with ditopic amines

To explore the halogen bonding to **25DIT** with heteroatom halogen bond acceptors, cocrystals with 4,4'-bipyridine (**4,4'-bipy**), 1,4-diazabicyclo[2.2.2]octane (**DABCO**), 1,2-Bis(2-pyridyl)ethylene (**dpe**), phenazine (**phenaz**), and tetramethylpyrazine (**Me_4pyrz**) were employed (Table 1 and Figure 2). The first four of these provided 1:1 cocrystals. Given the near-linear arrangement of iodine atoms in **25DIT**, the 1:1 cocrystals (**25DIT**)·(**4,4'-bipy**),

(**25DIT**)·(**DABCO**), (**25DIT**)·(**dpe**), and (**25DIT**)·(**phenaz**) display chains formed through I···N halogen bonding, with I···N distances ranging from 2.813(2) Å in (**25DIT**)·(**DABCO**) to 3.091(2) Å in (**25DIT**)·(**phenaz**).

This series of cocrystals provide a common halogen bonding motif, linear, 1:1 chains, to compare the interaction across common halogen bond donors. For example, with the non-fluorinated donor **I_2Bz**, its 1:1 **DABCO** cocrystal displays an I···N distance of 2.959(4) Å, an increase of approximately 0.15 Å relative to (**25DIT**)·(**DABCO**).[36,37] In contrast, the **I_2F_4Bz** and **I_2F_8bph** cocrystals with **DABCO** have I···N distances of 2.7350(8) Å and 2.6652(19) Å respectively, much shorter than in (**25DIT**)·(**DABCO**).[38] This highlights the correlation between maximum electrostatic potential and halogen bonding distance. The (**25DIT**)·(**phenaz**) chains have notable kinks, unlike the other three 1:1 cocrystals. This kinking is also observed in the (**I_2F_8bph**)·(**phenaz**) and (**Br_2F_8bph**)·(**phenaz**) cocrystals, so it does not appear to be attributed directly to the slight deviation from non-linearity of the iodine atoms in **25DIT** relative to benzene or biphenyl-based halogen bond donor. Neighboring kinked chains are consolidated through S···π interactions between **25DIT** molecules (3.5916(19) Å), as well as significant π···π interactions between neighboring **phenaz** molecules.

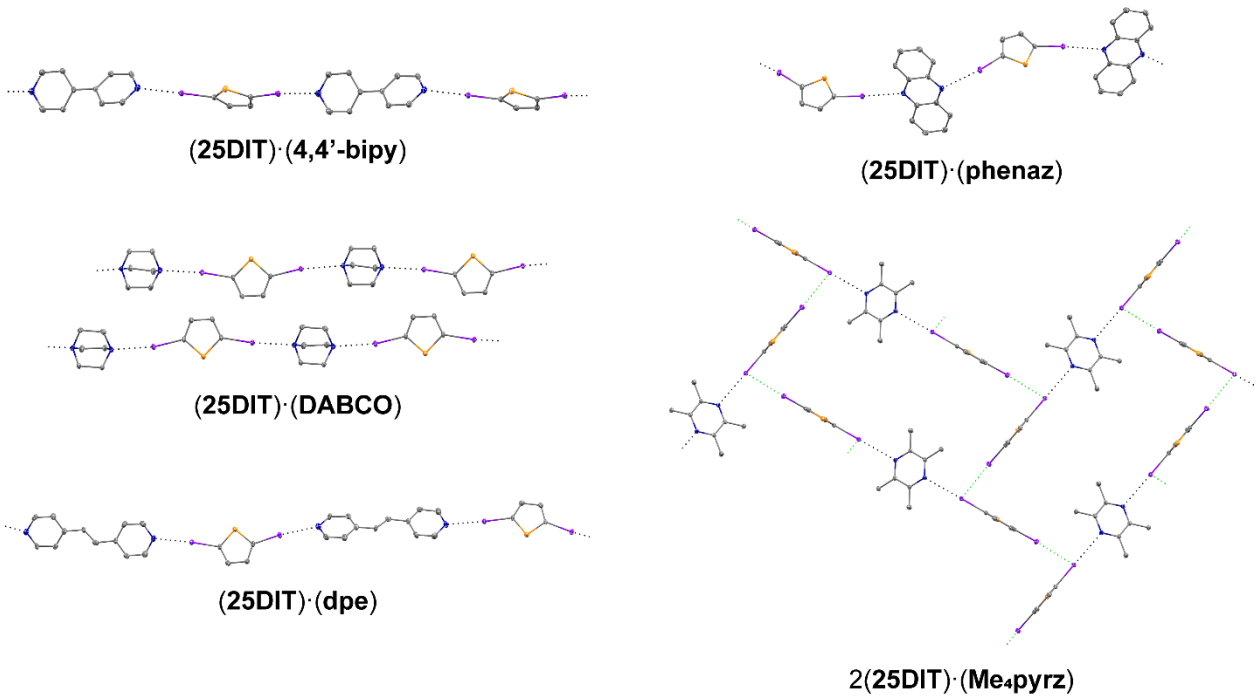

Figure 2. Halogen bonding in cocrystals of **25DIT** with various ditopic amines. Intermolecular I···N (black) and I···I (green) interactions are shown as dotted lines. Hydrogen atoms are omitted for clarity. Atomic displacement ellipsoids are shown at the 50% probability level.

In the case of **Me$_4$pyrz**, only the 2:1 cocrystal 2(**25DIT**)·(**Me$_4$pyrz**) was obtained. The second equivalent of **25DIT** allows for the formation of edge-sharing rings through halogen bonding, which consolidates into sheets in the (1 0 1) plane. This structure highlights the amphoteric nature of organoiodines in halogen bonding, with each iodine atom acting as a halogen bond donor to a nitrogen atom acceptor and a halogen bond acceptor to another C–I iodine atom. The I···N interaction is significantly shorter (3.0992(18) Å, R_{XB} = 0.84, R_{XB} = normalized halogen bond distance parameter) than the I···I one (3.8112(3) Å, R_{XB} = 0.93). Like in the **DABCO** cocrystals, the I···N distance in 2(**25DIT**)·(**Me$_4$pyrz**) is longer than in (**I$_2$F$_4$Bz**)·(**Me$_4$pyrz**) (3.0665(18) Å) and (**I$_2$F$_8$bph**)·(**Me$_4$pyrz**) (3.0187(19) Å), but shorter than in (**I$_2$Bz**)·(**Me$_4$pyrz**) (3.297(4) Å).[39,40] The I···N distance in 2(**25DIT**)·(**Me$_4$pyrz**) is also the longest

of the five ditopic amine structures presented within this study. This distance is a function of both minimum electrostatic potential at the nitrogen atom and the steric environment around that nitrogen atom and fall along previously determined trends.[37]

Table 1. Selected halogen bond parameters (Å, °) for cocrystals with ditopic amine halogen bond acceptors

Cocrystal	*I*···*A*	$d_{I\cdots A}$	R_{XB}[a]	$\theta_{C-I\cdots A}$	$\theta_{I\cdots N\cdots Y}$[b]
(**25DIT**)·(**4,4'-bipy**)	I1···N1	2.8577(17)	0.77	176.91(6)	169.76(8)
	I2···N2	2.9148(19)	0.78	172.13(6)	172.60(7)
(**25DIT**)·(**DABCO**)	I1···N1	2.828(2)	0.76	169.53(8)	174.10(9)
	I2···N2	2.813(2)	0.76	173.30(6)	176.96(11)
	I3···N3	2.814(2)	0.76	173.58(6)	179.11(12)
	I4···N4	2.833(2)	0.77	170.36(7)	172.62(7)
(**25DIT**)·(**dpe**)	I1···N1	2.861(5)	0.77	176.25(16)	170.4(2)
	I2···N2	2.937(5)	0.79	173.80(18)	163.2(2)
(**25DIT**)·(**phenaz**)	I1···N1	3.055(2)	0.83	175.21(8)	176.65(10)
	I2···N2	3.091(2)	0.84	168.70(8)	146.02(9)
2(**25DIT**)·(**Me$_4$pyrz**)[c]	I1···I2	3.8112(3)	0.93	174.79(5)	–
	I2···N1	3.0992(18)	0.84	178.46(6)	158.08(11)

[a]R_{XB} = $d_{I\cdots A}/\sum d_{Vdw}$, the ratio of the distance between the donor atom (i.e., I) and the acceptor atom (i.e., N) to the sum of their van der Waals radii (N, 1.66 Å; I, 2.04 Å).[41] [b]Angle defined by the iodine atom of the halogen bond, the nitrogen atom of the halogen bond, and the *para* carbon atom (**4,4'-bipy** and **dpe**) or opposite nitrogen atom (**DABCO**, **phenaz**, and **Me$_4$pyrz**). [c] $\theta_{C-A\cdots I}$ = 80.91(5)° and $\theta_1 - \theta_2$ =93.88(10)°, where $\theta_1 - \theta_2 = [(\theta_{C-I\cdots A}) - (\theta_{C-A\cdots I})]$

Cocrystals with ammonium and phosphonium iodide and triiodide salts

When cocrystallized with various tetraalkyl/aryl ammonium and phosphonium iodide salts, a diversity of halogen bonding motifs was observed, including 0-dimensional, discrete halogen bonding units, 1-dimensional chains, and 2-dimensional sheets (Table 2). In some cases, multiple cocrystalline stoichiometries were accessible from the same iodide salt, with this change

in stoichiometry resulting in a change in the halogen bonding motif. Of the 14 structures obtained utilizing iodide or triiodide salts, five, which incorporate trimethylphenylammonium iodide (**NMe_3PhI**), trimethylbenzylammonium iodide (**NMe_3BzI**), N-methylbenzothiazolium iodide (**NMeBenzoSI**), tetrapropylammondium triiodide (**$NProp4I_3$**), and tributylbenzylammonium iodide (**$NBut_3BzI$**), display discrete halogen bonding units (Figure 3). Each of these cocrystals involves an ammonium iodide-rich stoichiometry. Three of these structures, (**25DIT**)·2(**NMe_3PhI**), (**25DIT**)·2(**NMe_3BzI**), and (**25DIT**)·2(**NMeBenzoSI**), display a discrete halogen bonding unit consisting of one **25DIT** molecule with halogen bonds from both C–I iodine atoms to an iodide anion. These halogen bonds are all of a similar distance, with R_{XB} ranging from 0.85 to 0.87. The addition of molecular diiodine, I_2, to the reaction of **25DIT** and tetrapropylammonium iodide (**$NProp_4I$**) resulted in the (**25DIT**)·2(**$NProp_4I_3$**) cocrystal. A similar discrete unit is observed with the same 1:2 stoichiometry as the previous three cocrystals, with a single **25DIT** molecule pinned between two I_3^- anions. Each C–I iodine atom is involved (as the halogen bond donors) in halogen bonds to both the central and a terminal iodine atom of an I_3^- unit (as the halogen bond acceptors), with the I···I distances being significantly longer than in the previously mentioned iodide units, with R_{XB} ranging from 0.93 to 1.00. Finally, with a 3:4 stoichiometry, the 3(**25DIT**)·4(**$NBut_3BzI$**) cocrystal displays discrete halogen bonding units consisting of three **25DIT** molecules and four iodide anions. The I···I distances are similar to the other iodide salts (R_{XB} = 0.86–0.88), with I···I···I angles of 114.373(17)° and 118.860(17)°.

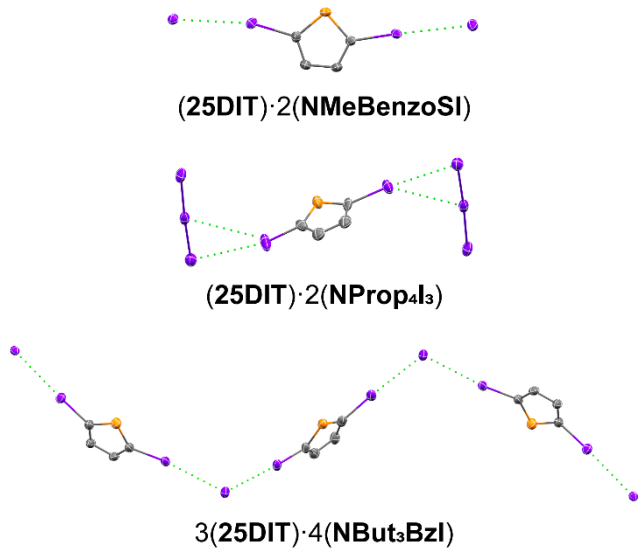

Figure 3. Representative examples of **25DIT** cocrystals containing discrete units. Intermolecular I···I (green) interactions are shown as dotted lines. Hydrogen atoms and cations are omitted for clarity. Atomic displacement ellipsoids are shown at the 50% probability level.

In five cocrystals obtained with 1:1 stoichiometry, involving salt components of tetrapentylammonium iodide (**$NPent_4I$**), tetrahexylammonium iodide (**$NHex_4I$**), 2-chloro-N-methylpyridinium iodide (**2-ClNMePyrI**), trimethylphenylammonium triiodide (**NMe_3PhI_3**), and trimethylbenzylammonium triiodide (**NMe_3BzI_3**), chains are formed via halogen bonding, much like the 1:1 chains formed with the ditopic amines (Figure 4). In the three iodide-containing structures, (**25DIT**)·(**$NPent_4I$**), (**25DIT**)·(**$NHex_4I$**), and (**25DIT**)·(**2Cl-NMePyrI**)·(**MeCN**), the resulting chains are parallel to one another in the structure. In the latter example, one of the two crystallographic unique chains has pendant 2Cl-NMePyr$^+$ cations, linked to the iodide anions via C–Cl···I halogen bonding (Cl···I = 3.5893(9) Å, R_{XB} =0.93). The orientation of the C–Cl bond along the second unique chain does not permit halogen bonding, and this cation instead primarily participates in a series of weak C–I···H interactions. The two 1:1 cocrystals containing a triiodide anion, (**25DIT**)·(**NMe_3PhI_3**) and (**25DIT**)·(**NMe_3BzI_3**), arrange into stepped chains, with both

terminal iodine atoms of the triiodide anion acting as halogen bond acceptors. The C–I···I distance ranges from 3.6003(4) Å to 3.7395(4) Å in these two triiodide salts, which is considerably longer than the 3.4891(4) Å in the chains of (**I2F4Bz**)·(**PMePh$_3$I$_3$**).[18]

With a slight increase in **25DIT** relative to the iodide-containing component, the 3:2 cocrystal with tetraphenylphosphonium iodide (**PPh$_4$I**), 3(**25DIT**)·2(**PPh$_4$I**), displays halogen bonding chains, much like the 1:1 cocrystals. However, the chains are further linked by **25DIT** to form ribbons. Both C–I iodine atoms in the linking **25DIT** molecule act as halogen bond donors, with C–I iodine atoms in the chains acting as halogen bond acceptors in addition to their role as halogen bond donors with the iodide acceptors to propagate the chain. A second 3:2 cocrystal, 3(**25DIT**)·2(**NMeBenzoSI**), shows the most variety of I···X interactions in one structure of those presented in this study. At the core of the halogen bonding motif is a disordered **25DIT** molecule in which both ends can participate in C–I···I–C and C–I···S–C halogen/chalcogen bonding with a different, fully-ordered **25DIT** molecule. To both sides of the sulfur atom of this central **25DIT** molecule are two other **25DIT** molecules, linked by C–I···S halogen bonding. The combination of these interactions extends the halogen bond motif into ribbons propagating along the *a* axis. The remaining C–I iodine atom on the **25DIT** molecules outside the ribbons acts as a halogen bond donor towards an iodide anion. These pendant **25DIT**···I$^-$ moieties further reinforce the ribbons through C-H···I interactions with one another.

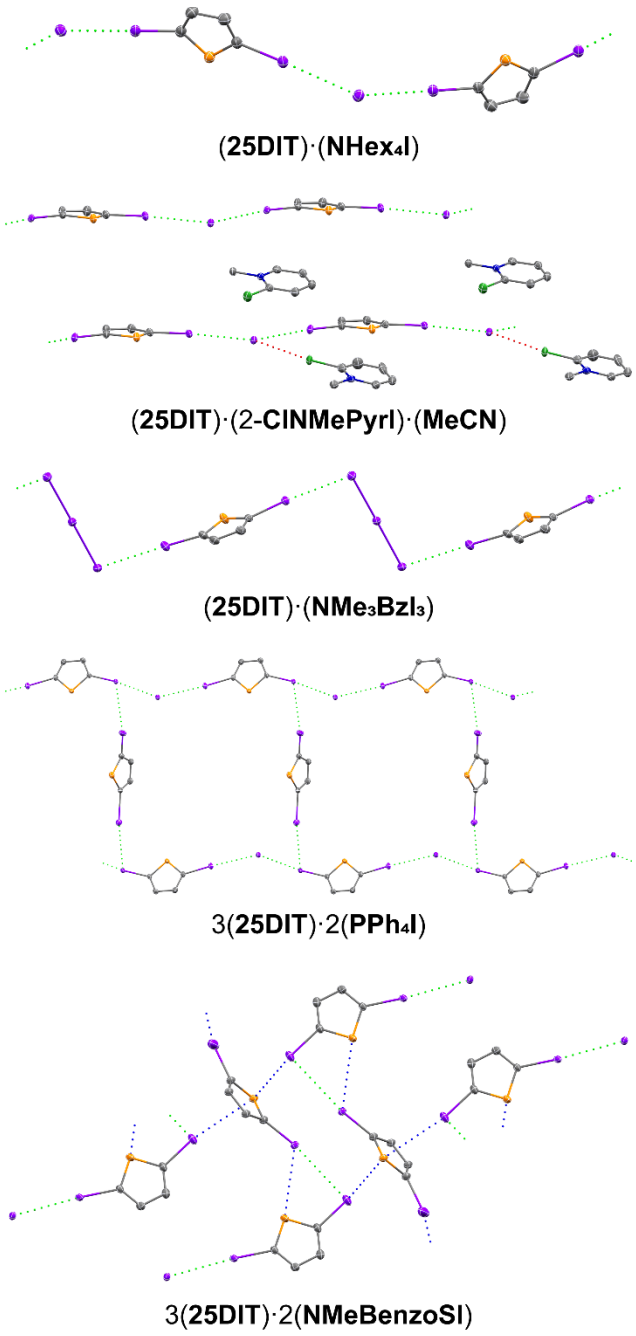

Figure 4. Representative examples of **25DIT** cocrystals containing chains and ribbons. Intermolecular I···I (green), I···S (blue), and Cl···I (red) interactions are shown as dotted lines. Hydrogen atoms and cations are omitted for clarity. Atomic displacement ellipsoids are shown at the 50% probability level.

The reactions with tetrapropylammonium iodide (**NProp$_4$I**) and tetrabutylammonium iodide (**NBut$_4$I**) produced the 2:1 cocrystals 2(**25DIT**)·(**NProp$_4$I**) and 2(**25DIT**)·(**NBut$_4$I**) respectively (Figure 5), further increasing the proportion of **25DIT**. In 2(**25DIT**)·(**NProp$_4$I**), a series of approximately linear chains along the *c* axis is formed via C–I···I···I–C halogen bonding, similar to the chains observed in the 1:1 cocrystals. The additional 25DIT molecule further links these chains by C–I···S and C–I···I halogen bonds, consolidating into sheets in the *bc* plane. The halogen bonding motif in 2(**25DIT**)·(**NBut$_4$I**) involves the formation of helical chains along the *c* axis constructed through C–I···I···I–C halogen bonding. Parallel chains are interconnected by the additional C–I iodine atom into sheets. Neighboring linking **25DIT** molecules are arranged to facilitate an S···S close contact (S···S = 3.666(2) Å, R_{XB} = 0.97). Secondary C–H···I interactions from **25DIT** to I^- anions connect neighboring sheets.

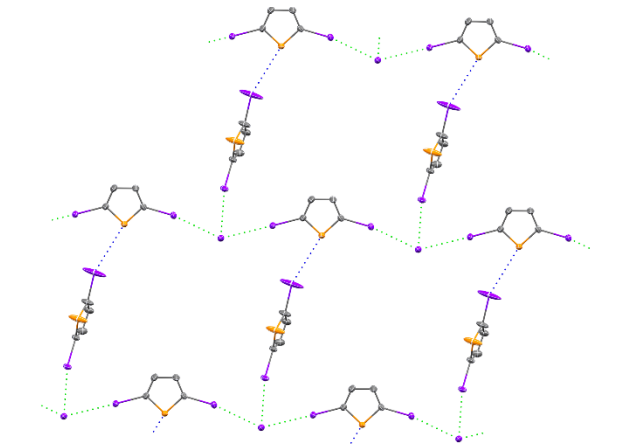

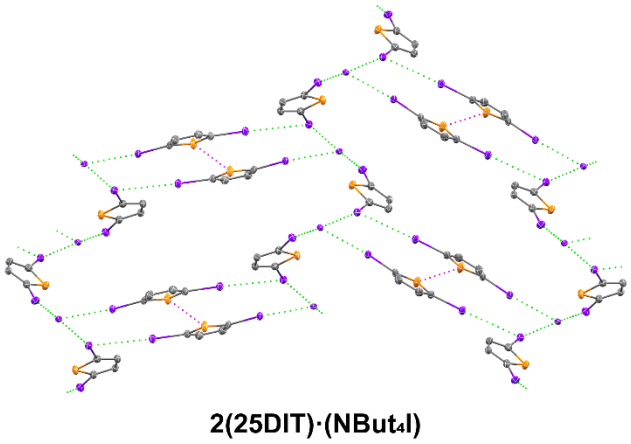

Figure 5. Representative examples of **25DIT** cocrystals containing sheets. Intermolecular I···I (green), I···S (blue), and S···S (magenta) interactions are shown as dotted lines. Hydrogen atoms and cations are omitted for clarity. Atomic displacement ellipsoids are shown at the 50% probability level.

Table 2. Selected halogen bond parameters (Å, °) for cocrystals with iodide and triiodide halogen bond acceptors

	Cocrystal	*I*···*A*	$d_{I\cdots A}$	R_{XB}[a]	$\theta_{C-I\cdots A}$	$\theta_{Y-A\cdots I}$	$\theta_1 - \theta_2$[b]	$\theta_{I\cdots I\cdots I}$
Discrete units	(**25DIT**)·2(**NMe_3PhI**)	I1···I3	3.4691(6)	0.85	171.97(9)	–	–	–
		I2···I4	3.5946(6)	0.88	165.5(1)	–	–	–
	(**25DIT**)·2(**NMe_3BzI**)	I1···I8	3.5294(7)	0.87	166.1(2)	–	–	–
		I2···I6	3.5494(6)	0.87	170.47(17)	–	–	–
		I3···I7	3.5688(5)	0.87	171.8(2)	–	–	–
		I4···I5	3.4654(7)	0.85	177.25(16)	–	–	–
	(**25DIT**)·2(**NMeBenzoSI**)	I1···I5	3.5575(4)	0.87	165.64(14)	–	–	–
		I2···I6	3.4672(4)	0.85	174.80(15)	–	–	–
		I3···I7	3.610(6)	0.88	161.2(4)	–	–	–
		I4···I7	3.511(6)	0.86	166.2(4)	–	–	–
	(**25DIT**)·2(**$NProp_4I_3$**)	I1···I3A	4.021(4)	0.99	138.3(4)	70.00(12)	68.3(5)	–
		I1···I4A	4.085(5)	1.00	130.8(4)	67.69(12)	63.1(5)	–
		I2···I3B	3.953(9)	0.97	163.0(4)	64.8(2)	98.2(6)	–
		I2···I4B	3.781(8)	0.93	148.9(4)	71.1(2)	77.8(6)	–
	3(**25DIT**)·4(**$NBut_3BzI$**)	I1···I5	3.5791(5)	0.88	169.29(12)	–	–	114.373(17) [I1···I5···I3]
		I3···I5	3.4983(6)	0.86	176.7(3)	–	–	118.860(17) [I1···I5···I4]
		I4···I5	3.5089(6)	0.86	174.5(2)	–	–	
		I2···I6	3.5250(5)	0.86	173.69(11)	–	–	–
chains	(**25DIT**)·(**$NPent_4I$**)[c]	I1···I6	3.5939(13)	0.88	172.3(4)	–	–	159.85(6)
		I5A···I6	3.527(3)	0.86	176.3(6)	–	–	
		I2···I3	3.5652(13)	0.87	171.9(3)	–	–	160.61(9)
		I1···I6	3.5939(13)	0.88	172.3(4)	–	–	
	(**25DIT**)·(**$NHex_4I$**)	I1···I2	3.4879(6)	0.85	178.53(14)	–	–	141.381(16)
	(**25DIT**)·(**2Cl-NMePyrI**)·(**MeCN**)	I1···I3	3.5850(4)	0.88	172.29(8)	–	–	156.110(15)
		I2···I3	3.5961(4)	0.88	172.32(8)	–	–	
		I4···I6	3.5809(4)	0.88	174.28(8)	–	–	
		I5···I6	3.5792(4)	0.88	170.42(9)	–	–	158.452(15)
		I4A···I3	3.528(3)	0.86	165.9(5)	–	–	
	(**25DIT**)·(**NMe_3PhI_3**)	I1···I3	3.7395(4)	0.92	165.3(3)	90.06(2)	75.24(5)	–
		I2···I5	3.6087(9)	0.88	167.2(3)	81.64(2)	85.56(5)	–
	(**25DIT**)·(**NMe_3BzI_3**)	I1···I3	3.6003(4)	0.88	175.21(8)	101.205(10)	73.96(9)	–
		I2···I5	3.6263(4)	0.89	169.75(8)	96.553(9)	73.20(9)	–
ribbons	3(**25DIT**)·2(**PPh_4I**)	I1···I5	3.5135(4)	0.86	173.16(5)	–	–	137.446(12)
		I2···I5	3.4732(4)	0.85	172.76(5)	–	–	
		I3···I2	4.0300(15)	0.99	170.43(14)	100.39(6)	70.0(2)	–
		I4···I2	3.7151(15)	0.91	159.33(16)	98.09(6)	61.2(2)	–
	3(**25DIT**)·2(**NMeBenzoSI**)[c]	I1···I3	3.4934(4)	0.86	175.98(11)	–	–	–
		I3A···I2	3.8255(15)	0.94	169.6(6)	89.22(12)	80.38(18)	–
		I2···S2A	3.705(15)	0.94	161.6(3)	88.1(8)	73.5(11)	–
		S1···I3A	3.727(2)	0.95	164.78(11)	120.0(6)	44.8(7)	–
		I4A···S1	3.527(3)	0.90	154.5(5)	141.86(12)	12.64(17)	–
sheets	2(**25DIT**)·(**$NProp_4I$**)	I1···I5	3.5582(11)	0.87	166.6(4)	–	–	73.91(3) [I1···I5···I3]
		I3···I5	3.4958(12)	0.86	170.7(3)	–	–	76.84(2) [I1···I5···I4]
		I4···I5	3.5313(11)	0.87	178.1(4)	–	–	137.69(3) [I3···I5···I4]
		I2···I4	4.0493(18)	0.99	147.7(5)	86.6(4)	61.1(9)	–
		I2···S2	3.747(3)	0.95	158.4(5)	102.1(4)	56.3(9)	–
		I1···I3	3.8438(9)	0.94	161.57(12)	89.72(11)	71.85(2)	–
	2(**25DIT**)·(**$NBut_4I$**)	I2···I9	3.4611(8)	0.85	175.18(11)	–	–	84.603(19) [I2···I9···I3]
		I3···I9	3.6006(8)	0.88	162.88(11)	–	–	69.800(17) [I3···I9···I4]
		I4···I9	3.6101(8)	0.88	167.77(10)	–	–	128.499(18) [I2···I9···I4]
		I5···I10	3.6648(8)	0.90	162.59(10)	–	–	66.899(16) [I5···I10···I6]
		I6···I10	3.7542(8)	0.92	147.11(11)	–	–	65.766(16) [I6···I10···I7]
		I7···I10	3.5649(8)	0.87	167.42(10)	–	–	132.281(18) [I5···I10···I7]
		I6···I7	3.9769(9)	0.97	157.96(11)	116.69(11)	41.3(2)	–
		I8···I6	3.8851(8)	0.95	161.23(12)	99.59(11)	61.6(2)	–

[a]R_{XB} = dI···A/∑dVdw, the ratio of the distance between the donor atom (i.e., I) and the acceptor atom (i.e., S, I) to the sum of their van der Waals radii (S, 1.89 Å; I, 2.04 Å).[41] [b]$\theta_1 - \theta_2 = [(\theta_{C–I···A}) - (\theta_{C–A···I})]$ [c] Only contacts involving the primary component of the disorder are tabulated.

Conclusions

Cocrystal stoichiometry is a significant driving factor in the dimensionality of the XB motif. Salt-rich 1:2 and 3:4 cocrystals formed 0-D discrete units, while 1:1 cocrystal stoichiometries resulted in single-stranded 1-D motifs. The ability of **25DIT** to act as both a donor and acceptor is shown in some instances to extend halogen bonded chains into ribbons or sheets. In this way, extension to organoiodine-rich cocrystals with 3:2 stoichiometry created double-stranded chains (or ribbons), and cocrystals with 2:1 stoichiometry resulted in 2-D sheets. The ditopic nitrogen acceptors formed similar XB motifs with **25DIT** as they did with their **I2F4Bz** counterparts in other studies, favoring 1:1 chains propagated by I···N halogen bonds. In these systems, I···I interactions only became operable when the cocrystal stoichiometry contained excess **25DIT**. The systems examined involving I- and I3- acceptors highly favor I···I halogen bonding (both between **25DIT** molecules and between **25DIT** molecules and I^- or I_3^- anions), and only in two instances was an I···S interaction operable. Having an intermediate electrostatic potential between **I_2Bz** and **I_2F_4Bz**, **25DIT** shows considerable versatility as a halogen bonding synthon. **25DIT** was shown to stabilize crystal packing through both I···S halogen and chalcogen bonds, along with S···S, S···π, and C–H···π interactions. These and related systems may be promising candidates for developing ionic liquids derived from ionic cocrystals or for further modification targeting deep eutectic solvent behavior.

ASSOCIATED CONTENT

Supporting Information. The following files are available free of charge.

Full experimental details of cocrystal synthesis and Crystallographic data and selected data collection parameters (PDF)

Accession Codes

CCDC 2112372–2112391 contain the supplementary crystallographic data for this paper. These data can be obtained free of charge via www.ccdc.cam.ac.uk/data_request/cif, or by emailing data_requests@ccdc.cam.ac.uk, or by contacting The Cambridge Crystallograhic Data Centre, 12 Union Road, Cambridge CB2 1EZ, UK; fax +44 1223 336033.

AUTHOR INFORMATION

Corresponding Author

Colin D. McMillen: e-mail, cmcmill@clemson.edu

William T. Pennington: e-mail, billp@clemson.edu

ORCID

Andrew J. Peloquin: 0000-0002-7535-2049

Colin D. McMillen: 0000-0002-7773-8797

William T. Pennington: 0000-0001-5224-7046

Author Contributions

The manuscript was written through contributions of all authors. All authors have given approval to the final version of the manuscript.

ACKNOWLEDGMENT

AJP acknowledges the United States Air Force Institute of Technology Civilian Institutions program and the Air Force Office of Scientific Research for fellowship support. The authors thank the NSF grants CHE-1560300 and CHE-2050042 for supporting this work. We also acknowledge Clemson University for the generous allotment of computational time on the Palmetto cluster.

REFERENCES

(1) Cavallo, G.; Metrangolo, P.; Milani, R.; Pilati, T.; Priimagi, A.; Resnati, G.; Terraneo, G. The Halogen Bond. *Chem. Rev.* **2016**, *116* (4), 2478–2601. https://doi.org/10.1021/acs.chemrev.5b00484.

(2) Vogel, L.; Wonner, P.; Huber, S. M. Chalcogen Bonding: An Overview. *Angew. Chemie - Int. Ed.* **2019**, *58* (7), 1880–1891. https://doi.org/10.1002/anie.201809432.

(3) Desiraju, G. R.; Shing Ho, P.; Kloo, L.; Legon, A. C.; Marquardt, R.; Metrangolo, P.; Politzer, P.; Resnati, G.; Rissanen, K. Definition of the Halogen Bond (IUPAC Recommendations 2013). *Pure Appl. Chem.* **2013**, *85* (8), 1711–1713. https://doi.org/10.1351/PAC-REC-12-05-10.

(4) Aakeroy, C. B.; Bryce, D. L.; Desiraju, G. R.; Frontera, A.; Legon, A. C.; Nicotra, F.; Rissanen, K.; Scheiner, S.; Terraneo, G.; Metrangolo, P.; et al. Definition of the Chalcogen Bond (IUPAC Recommendations 2019). *Pure Appl. Chem.* **2019**, *91* (11), 1889–1892. https://doi.org/10.1515/pac-2018-0713.

(5) Murray, J. S.; Lane, P.; Politzer, P. Expansion of the σ-Hole Concept. *J. Mol. Model.* **2009**, *15*, 723–729. https://doi.org/10.1007/s00894-008-0386-9.

(6) Politzer, P.; Murray, J. S. σ-Hole Interactions: Perspectives and Misconceptions. *Crystals*

2017, *7* (7), 212–226. https://doi.org/10.3390/cryst7070212.

(7) Politzer, P.; Murray, J. S.; Clark, T. Halogen Bonding and Other σ-Hole Interactions: A Perspective. *Phys. Chem. Chem. Phys.* **2013**, *15* (27), 11178–11189. https://doi.org/10.1039/c3cp00054k.

(8) Sirimulla, S.; Bailey, J. B.; Vegesna, R.; Narayan, M. Halogen Interactions in Protein-Ligand Complexes: Implications of Halogen Bonding for Rational Drug Design. *J. Chem. Inf. Model.* **2013**, *53* (11), 2781–2791. https://doi.org/10.1021/ci400257k.

(9) Wilcken, R.; Zimmermann, M. O.; Lange, A.; Zahn, S.; Kirchner, B.; Boeckler, F. M. Addressing Methionine in Molecular Design through Directed Sulfur-Halogen Bonds. *J. Chem. Theory Comput.* **2011**, *7* (7), 2307–2315. https://doi.org/10.1021/ct200245e.

(10) Ford, M. C.; Saxton, M.; Ho, P. S. Sulfur as an Acceptor to Bromine in Biomolecular Halogen Bonds. *J. Phys. Chem. Lett.* **2017**, *8* (17), 4246–4252. https://doi.org/10.1021/acs.jpclett.7b01725.

(11) Groom, C. R.; Bruno, I. J.; Lightfoot, M. P.; Ward, S. C. The Cambridge Structural Database. *Acta Crystallogr. Sect. B Struct. Sci. Cryst. Eng. Mater.* **2016**, *72* (2), 171–179. https://doi.org/10.1107/S2052520616003954.

(12) Kao, J.; Lilly, A. C. Theoretical Studies of Electronic Properties of Polyacene, Poly(1,4-Dihydrobenzo-1,4-Dihydrobenzene), Poly(p-Phenylene), and Poly(/7-1,4-Dihydrobenzene) and Their Hetero (N, O, and S) Substituted Derivatives. *J. Am. Chem. Soc.* **1987**, *109*, 4149–4157.

(13) Bryce, M. R.; Chesney, A.; Lay, A. K.; Batsanov, A. S.; Howard, J. A. K. New Pi-Electron Donor Systems Based on Accenapththo[1,2-b][1,4]-Dithinine. *J. Chem. Soc. - Perkin Trans. 1* **1996**, 2451–2459.

(14) Peintinger, M. F.; Beck, J.; Bredow, T. Charged Stacks of Dithiin, Diselenin, Thianthrene and Selenanthrene Radical Cations: Long Range Multicenter Bonds. *Phys. Chem. Chem. Phys.* **2013**, *15* (42), 18702–18709. https://doi.org/10.1039/c3cp53410c.

(15) Tomura, M.; Yamashita, Y. 4,5-Diiodo[1,2,5]Thiadiazolotetrathiafulvalene. *Acta Crystallogr. Sect. E Struct. Reports Online* **2004**, *60*, 63–65. https://doi.org/10.1107/S1600536803027466.

(16) Peloquin, A. J.; Kobra, K.; McMillen, C. D.; Iacono, S. T.; Pennington, W. T. Isolation of Hydrazine Oxidation Products via Halogen Bonding: C–I Bond Scission and Crystal Polymorphism . *CrystEngComm* **2021**, 419–426. https://doi.org/10.1039/d0ce01568g.

(17) Peloquin, A.; McMillen, C. D.; Iacono, S. T.; Pennington, W. T. Crystal Engineering Using Polyiodide Halogen and Chalcogen Bonding to Isolate the Phenothiazinium Radical Cation and Its Rare Dimer, 10-(3-phenothiazinylidene)Phenothiazinium. *Chem. – A Eur. J.* **2021**, *27*, 8398–8405. https://doi.org/10.1002/chem.202100730.

(18) Kobra, K.; O'Donnell, S.; Ferrari, A.; McMillen, C. D.; Pennington, W. T. Halogen Bonding and Triiodide Asymmetry in Cocrystals of Triphenylmethylphosphonium Triiodide with Organoiodines. *New J. Chem.* **2018**, *42* (13), 10518–10528. https://doi.org/10.1039/c8nj01373j.

(19) Peloquin, A. J.; Ragusa, A. C.; McMillen, C. D.; Pennington, W. T. The Reaction of Thiourea and 1,3-Dimethylthiourea towards Organoiodines: Oxidative Bond Formation and Halogen Bonding. *Acta Crystallogr. Sect. C Struct. Chem.* **2021**, *77*, 1–11. https://doi.org/10.1107/s205322962100869x.

(20) Peloquin, A. J.; McCollum, J. M.; McMillen, C. D.; Pennington, W. T. Halogen Bonding in Dithiane/Iodofluorobenzene Mixtures: A New Class of Hydrophobic Deep Eutectic

Solvents. *Angew. Chemie - Int. Ed.* **2021**, *80918*, 22983–22989. https://doi.org/10.1002/anie.202110520.

(21) Cheng, Y. J.; Yang, S. H.; Hsu, C. S. Synthesis of Conjugated Polymers for Organic Solar Cell Applications. *Chem. Rev.* **2009**, *109*, 5868–5923. https://doi.org/10.1021/cr900182s.

(22) Mazzio, K. A.; Luscombe, C. K. The Future of Organic Photovoltaics. *Chem. Soc. Rev.* **2015**, *44*, 78–90. https://doi.org/10.1039/c4cs00227j.

(23) Mishra, A.; Ma, C. Q.; Bäuerle, P. Functional Oligothiophenes: Molecular Design for Multidimensional Nanoarchitectures and Their Applications. *Chem. Rev.* **2009**, *109* (3), 1141–1176. https://doi.org/10.1021/cr8004229.

(24) Holdcroft, S. Patterning p -Conjugated Polymers. *Adv. Mater.* **2001**, *13* (23), 1753–1765.

(25) Cseh, L.; Mehl, G. H.; Clark, S.; Archibald, S. J. 3,4-Diiodo-2,5-Dimethylthiophene. *Acta Crystallogr. Sect. E Struct. Reports Online* **2007**, *63*, 1393–1394. https://doi.org/10.1107/S160053680700760X.

(26) Patel, D. G.; Sylvester, E. D.; LeValley, N. R.; Mitchell, T. B.; Benedict, J. B. The Structure and Characterization of 3,4,5-Triiodo-2-Methylthiophene: An Unexpected Iodination Product of 2-Methylthiophene. *J. Chem. Crystallogr.* **2019**, *49* (3), 206–212. https://doi.org/10.1007/s10870-019-00770-z.

(27) Parker, S. F.; Parker, J. L.; Jura, M. Structure and Vibrational Spectra of 2,5-Diiodothiophene: A Model for Polythiophene. *J. Phys. Chem. C* **2017**, *121* (23), 12636–12642. https://doi.org/10.1021/acs.jpcc.7b03803.

(28) APEX3; Bruker AXS: Madison, WI, USA, **2015**.

(29) Sheldrick, G. M. Crystal Structure Refinement with SHELXL. *Acta Crystallogr. Sect. C Struct. Chem.* **2015**, *71* (Md), 3–8. https://doi.org/10.1107/S2053229614024218.

(30) Dolomanov, O. V.; Bourhis, L. J.; Gildea, R. J.; Howard, J. A. K.; Puschmann, H. OLEX2: A Complete Structure Solution, Refinement and Analysis Program. *J. Appl. Crystallogr.* **2009**, *42* (2), 339–341. https://doi.org/10.1107/S0021889808042726.

(31) Bourhis, L. J.; Dolomanov, O. V.; Gildea, R. J.; Howard, J. A. K.; Puschmann, H. The Anatomy of a Comprehensive Constrained, Restrained Refinement Program for the Modern Computing Environment - Olex2 Dissected. *Acta Crystallogr. Sect. A* **2015**, *71*, 59–75. https://doi.org/10.1107/S2053273314022207.

(32) M. J. Frisch, G. W. Trucks, H. B. Schlegel, G. E. S.; M. A. Robb, J. R. Cheeseman, G. Scalmani, V. Barone, B. M.; G. A. Petersson, H. Nakatsuji, M. Caricato, X. Li, H. P. H.; A. F. Izmaylov, J. Bloino, G. Zheng, J. L. Sonnenberg, M. H.; M. Ehara, K. Toyota, R. Fukuda, J. Hasegawa, M. Ishida, T. N.; Y. Honda, O. Kitao, H. Nakai, T. Vreven, J. A. Montgomery, J.; J. E. Peralta, F. Ogliaro, M. Bearpark, J. J. Heyd, E. B.; K. N. Kudin, V. N. Staroverov, T. Keith, R. Kobayashi, J. N.; K. Raghavachari, A. Rendell, J. C. Burant, S. S. Iyengar, J. T.; M. Cossi, N. Rega, J. M. Millam, M. Klene, J. E. Knox, J. B. C.; et al. Gaussian 09 B.01. Gaussian, Inc.: Wallingford, CT 2010.

(33) Weigend, F. Accurate Coulomb-Fitting Basis Sets for H to Rn. *Phys. Chem. Chem. Phys.* **2006**, *8* (9), 1057–1065. https://doi.org/10.1039/b515623h.

(34) Weigend, F.; Ahlrichs, R. Balanced Basis Sets of Split Valence, Triple Zeta Valence and Quadruple Zeta Valence Quality for H to Rn: Design and Assessment of Accuracy. *Phys. Chem. Chem. Phys.* **2005**, *7* (18), 3297–3305. https://doi.org/10.1039/b508541a.

(35) Lu, T.; Chen, F. Multiwfn: A Multifunctional Wavefunction Analyzer. *J. Comput. Chem.* **2012**, *33* (5), 580–592. https://doi.org/10.1002/jcc.22885.

(36) Cinčić, D.; Friščič, T.; Jones, W. D. Structural Equivalence of Br and I Halogen Bonds: A

Route to Isostructural Materials with Controllable Properties. *Chem. Mater.* **2008**, *20*, 6623–6626. https://doi.org/10.1039/b003788p.

(37) Peloquin, A. J.; McMillen, C. D.; Pennington, W. T. One Dimensional Halogen Bond Design: Br···N versus I···N with Fluoroarenes. *CrystEngComm* **2021**, *23*, 6098–6106. https://doi.org/10.1039/d1ce00864a.

(38) Wang, R.; George, J.; Potts, S. K.; Kremer, M.; Dronskowski, R.; Englert, U. The Many Flavours of Halogen Bonds Message from Experimental Electron Density and Raman Spectroscopy. *Acta Crystallogr. Sect. C Struct. Chem.* **2019**, *75*, 1190–1201. https://doi.org/10.1107/S205322961901132X.

(39) Syssa-Magale, J. L.; Boubekeur, K.; Palvadeau, P.; Meerschaut, A.; Schöllhorn, B. The Tailoring of Crystal Structures via the Self-Assembly of Organic Coordination Compounds by N···I Non-Covalent Halogen Bonds: Co-Crystals of Sterically Hindered N-Heterocycles and 1,4-Diiodo-Tetrafluorobenzene. *CrystEngComm* **2005**, *7* (50), 302–308. https://doi.org/10.1039/b500009b.

(40) Szell, P. M. J.; Gabriel, S. A.; Caron-Poulin, E.; Jeannin, O.; Fourmigue, M.; Bryce, D. L. Cosublimation: A Rapid Route toward Otherwise Inaccessible Halogen-Bonded Architectures. *Cryst. Growth Des.* **2018**, *18* (10), 6227–6238. https://doi.org/10.1021/acs.cgd.8b01089.

(41) Alvarez, S. A Cartography of the van Der Waals Territories. *Dalt. Trans.* **2013**, *42* (24), 8617–8636. https://doi.org/10.1039/c3dt50599e.

For Table of Contents Use Only

2,5-Diiodothiophene: A Versatile Halogen Bonding Synthon for Crystal Engineering

Arianna C. Ragusa, Andrew J. Peloquin, Colin D. McMillen*, and William T. Pennington*

2,5-diiodothiophene

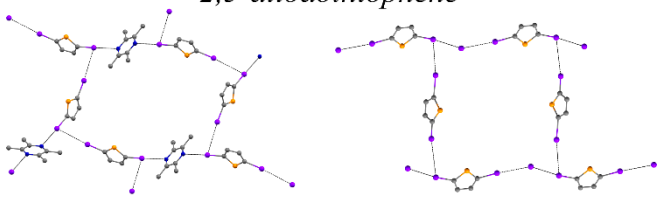

versatile halogen bond donor

The simple, commercially available organoiondine 2,5-diiodothiophene was utilized as a halogen bond donor with ditopic amines, ammonium iodides and triiodides, and tetraphenylphosphium iodide to provide 19 new crystal structures. These structures reveal a wide-range of packing motifs, marking this a versatile molecule in the halogen bonding "tool-box."

Supporting Information

2,5-Diiodothiophene: A Versatile Halogen Bonding Synthon for Crystal Engineering

Arianna C. Ragusa, Andrew J. Peloquin, Colin D. McMillen, and William T. Pennington

Department of Chemistry, Clemson University, Clemson, South Carolina (USA)

Table of Contents

Additional refinement details

In (**25DIT**)·2(**NMeBenzoSI**), (**25DIT**)·2(**NProp$_4$I$_3$**), 3(**25DIT**)·4(**NBut$_3$BzI**), and 3(**25DIT**)·2(**PPh$_4$I**), the atomic positions of at least one **25DIT** molecule are half occupied, with full occupancy achieved through inversion. Positional disorder of the alkyl chains in 3(**25DIT**)·4(**NBut$_4$BzI**) and 2(**25DIT**)·(**NProp$_4$I**), the iodine atom locations of the triiodide anion of (**25DIT**)·2(**NProp$_4$I$_3$**), methyl group orientation in (**25DIT**)·2(**NMeBenzoSI**), and position of one of the **25DIT** molecule in (**25DIT**)·(**NPent$_4$I**) was observed, and well-controlled with a combination of ISOR, SIMU, SADI, EADP, and/or EXYZ constraints/restraints as necessary.

Cocrystal synthesis

(25DIT)·(4,4'-bipy): In a 20 mL glass vial, 2,5-diiodothiophene (43 mg, 0.13 mmol) and 4,4'-bipyridine (20 mg, 0.13 mmol) were combined in methanol (5 mL) and vigorously stirred until all solids had dissolved. The solvent was then allowed to slowly evaporate under ambient conditions until crystalline material was observed. The vial was then sealed to cease evaporation and preserve sample purity. T_{melt} 102°C. T_{decomp} 215°C. Anal Calcd for $C_{14}H_{10}I_2N_2S$ (491.2): C, 34.17; H, 2.05; N, 5.96; S, 6.52; Found: C, 34.36; H, 2.09; N, 6.21; S, 6.51.

(25DIT)·(DABCO): In a 20 mL glass vial, 2,5-diiodothiophene (55 mg, 0.16 mmol) and 1,4-diazabicyclo[2.2.2]octane (18 mg, 0.16 mmol) were combined in acetonitrile (10 mL) and vigorously stirred until all solids had dissolved. The solvent was then allowed to slowly evaporate under ambient conditions until crystalline material was observed. The vial was then sealed to cease evaporation and preserve sample purity. T_{decomp} 147°C. Anal Calcd for $C_{20}H_{28}I_4N_2S_2$ (896.2): C, 26.80; H, 3.15; N, 6.25; S, 7.16; Found: C, 26.72; H, 3.35; N, 6.40; S, 7.31.

(25DIT)·(dpe): In a 20 mL glass vial, 2,5-diiodothiophene (40 mg, 0.12 mmol) and 1,2-di(4-pyridyl)ethylene (22 mg, 0.12 mmol) were combined in methanol (10 mL) and vigorously stirred until all solids had dissolved. The solvent was then allowed to slowly evaporate under ambient conditions until crystalline material was observed. The vial was then sealed to cease evaporation and preserve sample purity. T_{melt} 93°C. T_{decomp} 201°C. Anal Calcd for $C_{16}H_{12}I_2N_2S$ (518.2): C, 37.09; H, 2.33; N, 5.41; S, 6.19; Found: C, 37.32; H, 2.58; N, 5.38; S, 6.31.

(25DIT)·(phenaz): In a 20 mL glass vial, 2,5-diiodothiophene (37 mg, 0.11 mmol) and phenazine (20 mg, 0.11 mmol) were combined in methanol (5 mL) and vigorously stirred until all solids had dissolved. The solvent was then allowed to slowly evaporate under ambient conditions until crystalline material was observed. The vial was then sealed to cease evaporation and preserve sample purity. T_{melt} 68°C. T_{decomp} 122°C. Anal Calcd for $C_{16}H_{10}I_2N_2S$ (516.2): C, 37.23; H, 1.95; N, 5.43; S, 6.21; Found: C, 37.53; H, 2.29; N, 5.57; S, 5.90.

2(25DIT)·(Me$_4$pyrz): In a 20 mL glass vial, 2,5-diiodothiophene (79 mg, 0.24 mmol) and 2,3,5,6-tetramethylpyrazine (16 mg, 0.12 mmol) were combined in ethanol (5 mL) and vigorously stirred until all solids had dissolved. The solvent was then allowed to slowly evaporate under ambient conditions until crystalline material was observed. The vial was then sealed to cease evaporation and preserve sample purity. Reactions performed at 1:1 stoichiometry also provided the 2:1 cocrystal. T_{melt} 90°C. T_{decomp} 115°C. Anal Calcd for $C_{16}H_{16}I_4N_2S_2$ (808.1): C, 23.78; H, 2.00; N, 3.47; S, 7.94; Found: C, 23.68; H, 1.74; N, 3.45; S, 7.58.

(25DIT)·2(NMe$_3$PhI): In a 20 mL glass vial, 2,5-diiodothiophene (44 mg, 0.13 mmol) and trimethylphenyliodide (69 mg, 0.26 mmol) were combined in methanol (5 mL) and vigorously stirred until all solids had dissolved. The solvent was then allowed to slowly evaporate under ambient conditions until crystalline material was observed. The vial was then sealed to cease evaporation and preserve sample purity. T_{melt} 45°C. T_{decomp} 142°C. Anal Calcd for $C_{22}H_{30}I_4N_2S$ (862.2): C, 30.65; H, 3.51; N, 3.25; S, 3.72; Found: C, 31.00; H, 3.90; N, 3.36; S, 3.35.

(25DIT)·2(NMe$_3$BzI): In a 20 mL glass vial, 2,5-diiodothiophene (54 mg, 0.16 mmol) and trimethylbenzylammonium iodide (89 mg, 0.32 mmol) were combined in ethanol (5 mL) and vigorously stirred until all solids had dissolved. The solvent was then allowed to slowly evaporate under ambient conditions until crystalline material was observed. The vial was then sealed to cease evaporation and preserve sample purity. T_{melt} 70°C. T_{decomp} 119°C. Anal Calcd for $C_{48}H_{68}I_8N_4S_2$ (1780.5): C, 32.38; H, 3.85; N, 3.15; S, 3.60; Found: C, 32.47; H, 3.66; N, 3.15; S, 3.25.

(25DIT)·2(NMeBenzoSI): In a 20 mL glass vial, 2,5-diiodothiophene (50 mg, 0.15 mmol) and *N*-methylbenzothiazolium iodide (82 mg, 0.30 mmol) were combined in acetonitrile (5 mL) and vigorously stirred until all solids had dissolved. The solvent was then allowed to slowly evaporate under ambient conditions until crystalline material was observed. The vial was then sealed to cease evaporation and preserve sample purity. T_{melt} 186°C. T_{decomp} 139°C. Anal Calcd for $C_{60}H_{54}I_{12}N_6S_9$ (2670.6): C, 26.99; H, 2.04; N, 3.15; S, 10.81; Found: C, 26.90; H, 2.10; N, 3.00; S, 10.68.

(25DIT)·2(NProp$_4$I$_3$): 2,5-diiodothiophene (48 mg, 0.14 mmol), tetrapropylammonium iodide (90 mg, 0.29 mmol), and diiodine (73 mg, 0.29 mmol) were subjected to mechanochemical grinding for 5 minutes. The resulting powder was dissolved in methanol (5 mL) and vigorously stirred until all solids had dissolved. The solvent was then allowed to slowly evaporate under ambient conditions until crystalline material was observed. The vial was then sealed to cease evaporation and preserve sample purity T_{melt} 71°C. T_{decomp} 229°C. Anal. Calcd for $C_{28}H_{58}I_8N_2S$ (1470.1): C, 22.88; H, 3.98; N, 1.91; S, 2.18; Found: C, 22.51; H, 3.80; N, 1.51; S, 2.43.

3(25DIT)·4(NBut$_3$BzI): In a 20 mL glass vial, 2,5-diiodothiophene (47 mg, 0.14 mmol) and tributylbenzylammonium iodide (75 mg, 0.19 mmol) were combined in ethanol (5 mL) and vigorously stirred until all solids had dissolved. The solvent was then allowed to slowly evaporate under ambient conditions until crystalline material was observed. The vial was then sealed to cease evaporation and preserve sample purity. T_{melt} 114°C. T_{decomp} 182°C. Anal Calcd for $C_{88}H_{134}I_{10}N_4S_3$ (2613.3): C, 40.45; H, 5.17; N, 2.14; S, 3.68; Found: C, 40.73; H, 5.23; N, 1.94; S, 3.60.

(25DIT)·(NPent$_4$I): In a 20 mL glass vial, 2,5-diiodothiophene (38 mg, 0.11 mmol) and tetrapentylammonium iodide (48 mg, 0.11 mmol) were combined in methanol (5 mL) and vigorously stirred until all solids had dissolved. The solvent was then allowed to slowly evaporate under ambient conditions until crystalline material was observed. The vial was then sealed to cease evaporation and preserve sample purity. T_{melt} 96°C. T_{decomp} 67°C. Anal Calcd for $C_{24}H_{46}I_3NS$ (761.4): C, 37.86; H, 6.09; N, 1.84; S, 4.21; Found: C, 37.77; H, 6.40; N, 1.59; S, 4.27.

(25DIT)·(NHex$_4$I): 2,5-diiodothiophene (55 mg, 0.16 mmol) and tetrahexylammonium iodide (79 mg, 0.16 mmol) were subjected to mechanochemical grinding for 5 minutes. The resulting powder was dissolved in methanol (5 mL) and vigorously stirred until all solids had dissolved. The solvent was then allowed to slowly evaporate under ambient conditions until crystalline material was observed. The vial was then sealed to cease evaporation and preserve sample purity. T_{melt} 93°C. T_{decomp} 140°C. Anal Calcd for $C_{28}H_{52}I_3NS$ (815.5): C, 41.24; H, 6.43; N, 1.72; S, 3.93; Found: C, 41.28; H, 6.73; N, 1.53; S, 3.60.

(25DIT)·(2Cl-NMePyrI)·(MeCN): In a 20 mL glass vial, 2,5-diiodothiophene (51 mg, 0.15 mmol) and 2-chloro-*N*-methylpyridinium iodide (39 mg, 0.15 mmol) were combined in acetonitrile (5 mL) and vigorously stirred until all solids had dissolved. The solvent was then allowed to slowly evaporate under ambient conditions until crystalline material was observed. The vial was then sealed to cease evaporation and preserve sample purity. The crystals did not posses sufficient stability to solvent loss for thermal or elemental analysis.

(25DIT)·(NMe$_3$PhI$_3$): 2,5-diiodothiophene (44 mg, 0.13 mmol), trimethylphenylammonium iodide (34 mg, 0.13 mmol), and diiodine (33 mg, 0.13 mmol) were subjected to mechanochemical grinding for 5 minutes. The resulting powder was dissolved in methanol (5 mL) and vigorously stirred until all solids had dissolved. The solvent was then allowed to slowly evaporate under ambient conditions until crystalline

material was observed. The vial was then sealed to cease evaporation and preserve sample purity. T_{melt} 111°C. T_{decomp} 150°C. Anal Calcd for $C_{13}H_{16}I_5NS$ (852.9): C, 18.31; H, 1.89; N, 1.64; S, 3.76; Found: C, 18.37; H, 1.71; N, 1.77; S, 4.05.

(25DIT)·(NMe_3BzI_3): 2,5-diiodothiophene (54 mg, 0.16 mmol), trimethylbenzylammonium iodide (45 mg, 0.16 mmol), and diiodine (41 mg, 0.16 mmol) were subjected to mechanochemical grinding for 5 minutes. The resulting powder was dissolved in methanol (5 mL) and vigorously stirred until all solids had dissolved. The solvent was then allowed to slowly evaporate under ambient conditions until crystalline material was observed. The vial was then sealed to cease evaporation and preserve sample purity. T_{melt} 74°C. T_{decomp} 156°C. Anal Calcd for $C_{14}H_{18}I_5NS$ (866.9): C, 19.40; H, 2.09; N, 1.62; S, 3.70; Found: C, 19.44; H, 2.43; N, 1.24; S, 3.71.

3(25DIT)·2(PPh_4I): In a 20 mL glass vial, 2,5-diiodothiophene (62 mg, 0.18 mmol) and tetraphenylphosphium iodide (57 mg, 0.12 mmol) were combined in acetonitrile (5 mL) and vigorously stirred until all solids had dissolved. The solvent was then allowed to slowly evaporate under ambient conditions until crystalline material was observed. The vial was then sealed to cease evaporation and preserve sample purity. T_{melt} 142°C. T_{decomp} 150°C. Anal Calcd for $C_{60}H_{46}I_8P_2S_3$ (1940.4): C, 37.14; H, 2.39; S, 4.96; Found: C, 37.10; H, 2.67; S, 4.60.

3(25DIT)·2(NMeBenzoSI): In a 20 mL glass vial, 2,5-diiodothiophene (58 mg, 0.17 mmol) and *N*-methylbenzothiazolium (32 mL, 0.12 mmol) were combined in ethanol (5 mL) and vigorously stirred until all solids had dissolved. The solvent was then allowed to slowly evaporate under ambient conditions until crystalline material was observed. The vial was then sealed to cease evaporation and preserve sample purity. T_{melt} 95°C. T_{decomp} 163°C. Anal Calcd for $C_{28}H_{22}I_8N_2S_5$ (1562.1): C, 21.53; H, 1.42; N, 1.79; S, 10.26; Found: C, 21.63; H, 1.55; N, 1.40; S, 10.43.

2(25DIT)·($NProp_4I$): In a 20 mL glass vial, 2,5-diiodothiophene (49 mg, 0.15 mmol) and tetrapropylammonium iodide (23 mg, 0.073 mmol) were combined in methanol (5 mL) and vigorously stirred until all solids had dissolved. The solvent was then allowed to slowly evaporate under ambient conditions until crystalline material was observed. The vial was then sealed to cease evaporation and preserve sample purity. T_{melt} 131°C. T_{decomp} 204°C. Anal Calcd for $C_{20}H_{28}I_5NS_2$ (981.1): C, 25.49; H, 2.88; N, 1.43; S, 6.54; Found: C, 25.72; H, 3.17; N, 1.72; S, 6.21.

2(25DIT)·($NBut_4I$): In a 20 mL glass vial, 2,5-diiodothiophene (43 mg, 0.13 mmol) and tetrabutylammonium iodide (24 mg, 0.064 mmol) were combined in methanol (5 mL) and vigorously stirred until all solids had dissolved. The solvent was then allowed to slowly evaporate under ambient conditions until crystalline material was observed. The vial was then sealed to cease evaporation and preserve sample purity. T_{melt} 115°C. T_{decomp} 200°C. Anal Calcd for $C_{24}H_{40}I_5NS_2$ (1041.2): C, 27.69; H, 3.87; N, 1.35; S, 6.16; Found: C, 27.73; H, 3.82; N, 1.54; S, 5.81.

Table SI1. Crystallographic data and selected data collection parameters

Cocrystal	**25DIT**	(**25DIT**)·(**4,4'-bipy**)	(**25DIT**)·(**DABCO**)	(**25DIT**)·(**dpe**)	(**25DIT**)·(**phenz**)	2(**25DIT**)·(**Me$_4$pyrz**)	(**25DIT**)·2(**NMe$_3$PhI**)
Empirical formula	$C_4H_2I_2S$	$C_{14}H_{10}I_2N_2S$	$C_{20}H_{28}I_4N_4S_2$	$C_{16}H_{12}I_2N_2S$	$C_{16}H_{10}I_2N_2S$	$C_{16}H_{16}I_4N_2S_2$	$C_{22}H_{30}I_4N2_S$
Formula weight (g/mol)	335.92	492.10	896.18	518.14	516.12	808.03	862.14
Crystal system	orthorhombic	triclinic	triclinic	monoclinic	monoclinic	monoclinic	monoclinic
Space group	*Pbca*	*P*-1	*P*-1	*P*2$_1$/*c*	*P*2$_1$/*n*	*P*2$_1$/*n*	*P*2$_1$/*n*
T (K)	115.03	99.99	99.99	100.0	99.99	100.0	100.0
a (Å)	5.2347(3)	8.5771(6)	9.6075(5)	9.1175(4)	4.2671(3)	9.5738(6)	18.2142(8)
b (Å)	14.9231(8)	9.8008(7)	10.4733(6)	9.3771(4)	28.4925(18)	9.2902(6)	8.6667(3)
c (Å)	18.2289(11)	10.3131(7)	14.8059(8)	19.3091(9)	13.3702(8)	12.7048(8)	19.3384(9)
α (°)	90	106.717(2)	84.886(2)	90	90	90	90
β (°)	90	96.718(3)	80.061(2)	96.8547(18)	95.415(2)	103.047(2)	116.249(2)
γ (°)	90	109.143(2)	63.850(2)	90	90	90	90
V (Å^3)	1424.00(14)	762.70(9)	1317.10(13)	1639.04(13)	1618.30(18)	1100.83(12)	2737.9(2)
ρ_{calcd} (g·cm^{-3})	3.134	2.143	2.260	2.100	2.118	2.438	2.092
reflns collected	8696	24056	53552	10532	34259	23606	49824
Independent reflns	1468	4448	6272	3233	4364	2490	5664
R(int)	0.0266	0.0305	0.0388	0.0560	0.0477	0.0307	0.0516
# parameters	64	172	271	190	190	111	268
R_1 [$I>2\sigma(I)$]	0.0147	0.0169	0.0172	0.0346	0.0219	0.0156	0.0217
wR_2 [$I>2\sigma(I)$]	0.0338	0.0379	0.0389	0.0575	0.0444	0.0379	0.0410
R_1 (all)	0.0165	0.0203	0.0206	0.0531	0.0279	0.0161	0.0294
wR_2 (all)	0.0347	0.0402	0.0405	0.0630	0.0480	0.0382	0.0460
GooF	1.127	1.128	1.088	1.044	1.161	1.227	1.253
Flack parameter	N/A	N/A	N/A	N/A	N/A	N/A	N/A
Largest diff. peak/hole (e Å^{-3})	0.47/-0.54	0.58/-0.48	0.74/-0.96	0.71/-1.05	0.54/-0.84	0.46/-0.78	1.08/-0.62
CCDC #	2112372	2112373	2112374	2112375	2112376	2112377	2112378

Table SI1 (cont). Crystallographic data and selected data collection parameters

Cocrystal	(**25DIT**)· 2(**NMe_3Bzl**)	(**25DIT**)· 2(**NMeBenzoSI**)	(**25DIT**)· 2(**$NProp_4I_3$**)	3(**25DIT**)· 4(**$NBut_3Bzl$**)	(**25DIT**)· (**$NPent_4I$**)	(**25DIT**)· (**$NHex_4I$**)	(**25DIT**)· (**2Cl-NMePyrI**)· (**MeCN**)
Empirical formula	$C_{48}H_{68}I_8N_4S_2$	$C_{60}H_{54}I_{12}N_6S_9$	$C_{28}H_{58}I_8N_2S$	$C_{88}H_{134}I_{10}N_4S_3$	$C_{24}H_{46}I_3NS$	$C_{28}H_{52}I_3NS$	$C_{12}H_{12}ClI_3N_2S$
Formula weight (g/mol)	1780.38	2670.43	1470.02	2613.16	761.38	815.46	632.45
Crystal system	triclinic	triclinic	monoclinic	triclinic	triclinic	tetragonal	monoclinic
Space group	*P*-1	*P*-1	*C*2/*c*	*P*-1	*P*-1	*I*-4*c*2	*P*2/*n*
T (K)	100.01	100.0	100.0	99.99	100.0	100.0	100.0
a (Å)	9.4720(6)	9.4761(6)	16.2946(10)	12.0622(6)	15.1881(17)	16.7256(17)	13.8452(7)
b (Å)	17.4002(11)	12.6494(8)	8.9179(5)	15.6635(6)	15.3022(17)	16.7256(17)	13.5301(7)
c (Å)	19.5476(12)	17.8953(11)	32.022(2)	15.8586(8)	17.4545(19)	24.883(2)	19.7216(9)
α (°)	96.203(2)	108.591(2)	90	70.222(2)	115.397(4)	90	90
β (°)	103.779(2)	99.127(2)	103.525(2)	74.467(2)	90.173(4)	90	91.363(2)
γ (°)	100.552(2)	95.486(2)	90	70.253(2)	119.361(4)	90	90
V (Å^3)	3037.0(3)	1982.7(2)	4524.2(5)	2613.6(2)	3074.4(6)	6960.9(16)	3693.3(3)
ρ_{calcd} (g·cm^{-3})	1.947	2.236	2.158	1.660	1.645	1.556	2.275
reflns collected	46243	67157	39943	70606	114999	74533	64438
Independent reflns	13974	8122	5222	11984	12697	4678	7496
R(int)	0.0623	0.0275	0.0451	0.0435	0.0576	0.0451	0.0388
# parameters	571	456	240	628	569	151	347
R_1 [$I>2\sigma(I)$]	0.0467	0.0295	0.0325	0.0318	0.0693	0.0217	0.0258
wR_2 [$I>2\sigma(I)$]	0.1121	0.0700	0.0592	0.0609	0.1685	0.0580	0.0577
R_1 (all)	0.0666	0.0325	0.0486	0.0437	0.0769	0.0236	0.0283
wR_2 (all)	0.1316	0.0731	0.0705	0.0691	0.1738	0.0602	0.0593
GooF	1.068	1.100	1.141	1.126	1.271	1.171	1.253
Flack parameter	N/A	N/A	N/A	N/A	N/A	0.001(8)	N/A
Largest diff. peak/hole (e Å^{-3})	1.08/-0.62	2.95/-1.15	1.01/-1.00	1.79/-1.70	2.86/-3.44	0.92/-0.51	1.25/-0.59
CCDC #	2112379	2112380	2112381	2112382	2112383	2112384	2112385

Table SI1 (cont). Crystallographic data and selected data collection parameters

Cocrystal	(**25DIT**)·(**NMe_3PhI_3**)	(**25DIT**)·(**NMe_3BzI_3**)	3(**25DIT**)·2(**PPh_4I**)	3(**25DIT**)·2(**NMeBenzoSI**)	2(**25DIT**)·(**$NProp_4I$**)	2(**25DIT**)·(**$NBut_4I$**)
Empirical formula	$C_{13}H_{16}I_5NS$	$C_{14}H_{18}I_5NS$	$C_{60}H_{46}I_8P_2S_3$	$C_{28}H_{22}I_8N_2S_5$	$C_{20}H_{28}I_5NS_2$	$C_{24}H_{40}I_5NS_2$
Formula weight (g/mol)	852.83	866.85	1940.29	1561.97	981.05	1041.19
Crystal system	triclinic	monoclinic	monoclinic	triclinic	triclinic	monoclinic
Space group	*P*-1	$P2_1/c$	$P2_1/c$	*P*-1	*P*-1	$P2_1/n$
T (K)	100.0	139.99	100.01	100.0	99.99	100.01
a (Å)	8.9740(8)	9.5804(6)	12.9651(4)	8.4098(7)	9.4288(6)	25.947(3)
b (Å)	9.6622(8)	18.0581(12)	15.5395(5)	9.1023(8)	12.8213(7)	9.2225(8)
c (Å)	13.0962(11)	13.0460(8)	15.8093(5)	13.9017(12)	13.0179(7)	28.598(3)
α (°)	80.915(3)	90	90	105.454(3)	105.130(2)	90
β (°)	74.815(3)	94.813(2)	100.5680(10)	99.616(3)	90.933(2)	93.572(4)
γ (°)	80.156(3)	90	90	92.986(3)	96.849(2)	90
V (Å^3)	1072.10(16)	2249.0(2)	3131.09(17)	1006.03(15)	1506.49(15)	6830.0(11)
ρ_{calcd} (g·cm^{-3})	2.642	2.560	2.058	2.578	2.163	2.025
reflns collected	19790	67667	50438	48994	47633	124325
Independent reflns	4189	6885	6368	5620	6927	16278
R(int)	0.0519	0.0442	0.0405	0.0426	0.0505	0.0674
# parameters	184	193	361	290	361	585
R_1 [$I>2\sigma(I)$]	0.0446	0.0245	0.0144	0.0326	0.0712	0.0293
wR_2 [$I>2\sigma(I)$]	0.1021	0.0453	0.0348	0.0708	0.1579	0.0508
R_1 (all)	0.0526	0.0326	0.0158	0.0338	0.0794	0.0443
wR_2 (all)	0.1055	0.0470	0.0357	0.0717	0.1631	0.0575
GooF	1.166	1.122	1.077	1.037	1.085	1.150
Flack parameter	N/A	N/A	N/A	N/A	N/A	N/A
Largest diff. peak/hole (e Å^{-3})	2.14/-1.35	0.72/-0.93	0.38/-0.33	5.49/-3.48	12.69/-10.65	2.37/-2.06
CCDC #	2112386	2112387	2112388	2112389	2112390	2112391

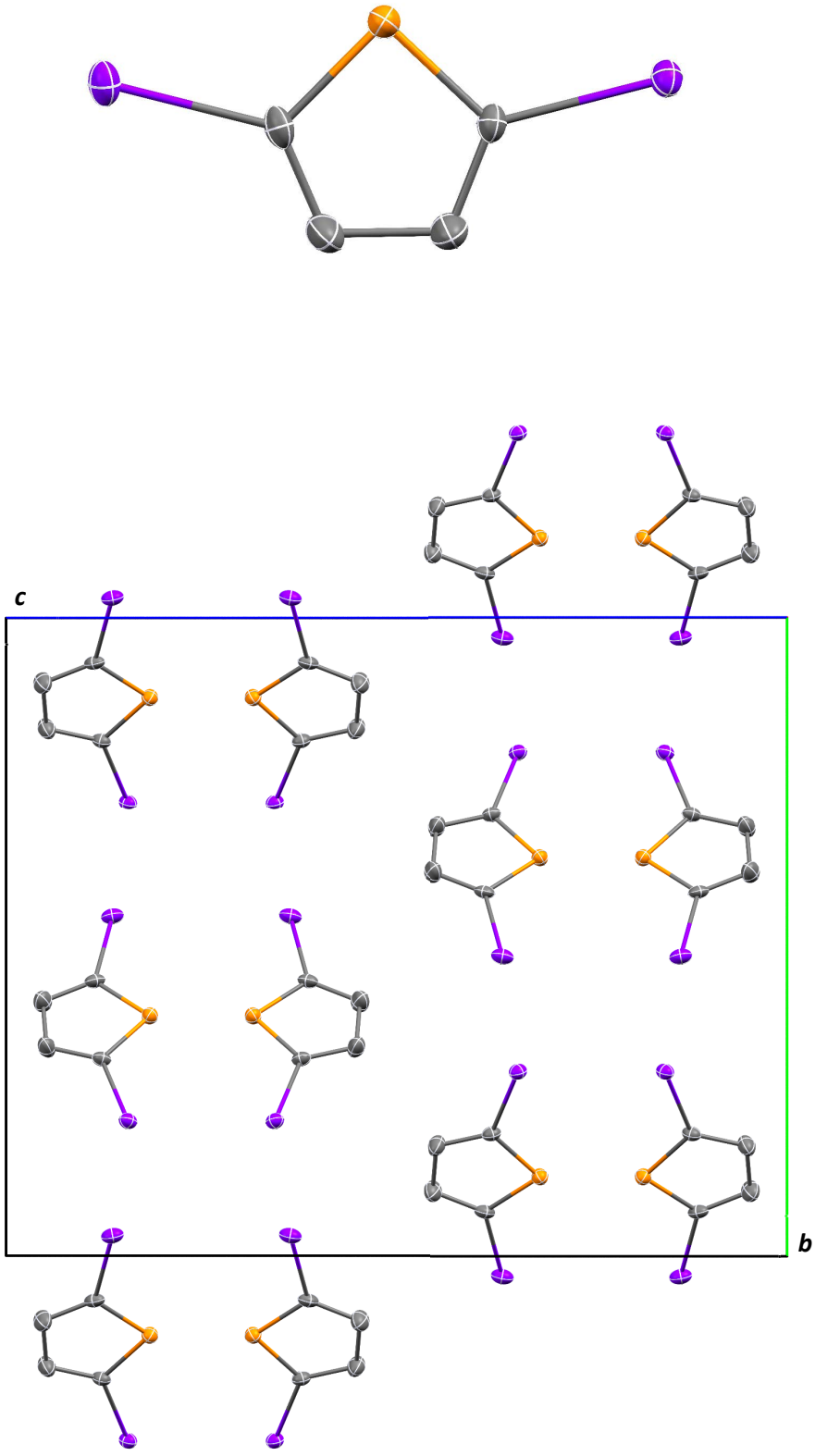

Figure SI1. Molecular structure (top) and unit cell packing (bottom) of **25DIT**. Hydrogen atoms are omitted for clarity. Atomic displacement ellipsoids are shown at the 50% probability level.

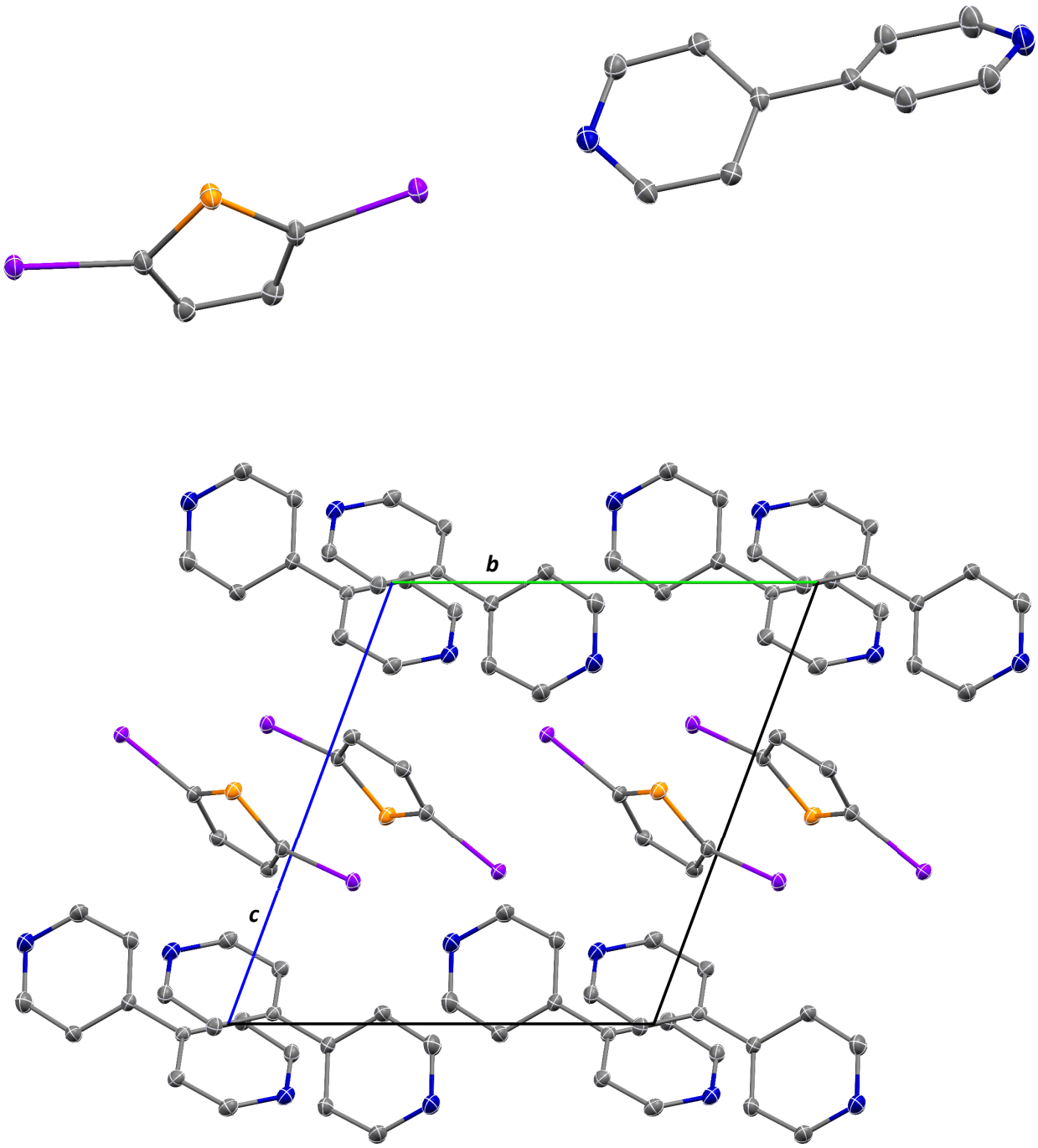

Figure SI2. Molecular structure (top) and unit cell packing (bottom) of (**25DIT**)·(**4,4'-bipy**). Hydrogen atoms are omitted for clarity. Atomic displacement ellipsoids are shown at the 50% probability level.

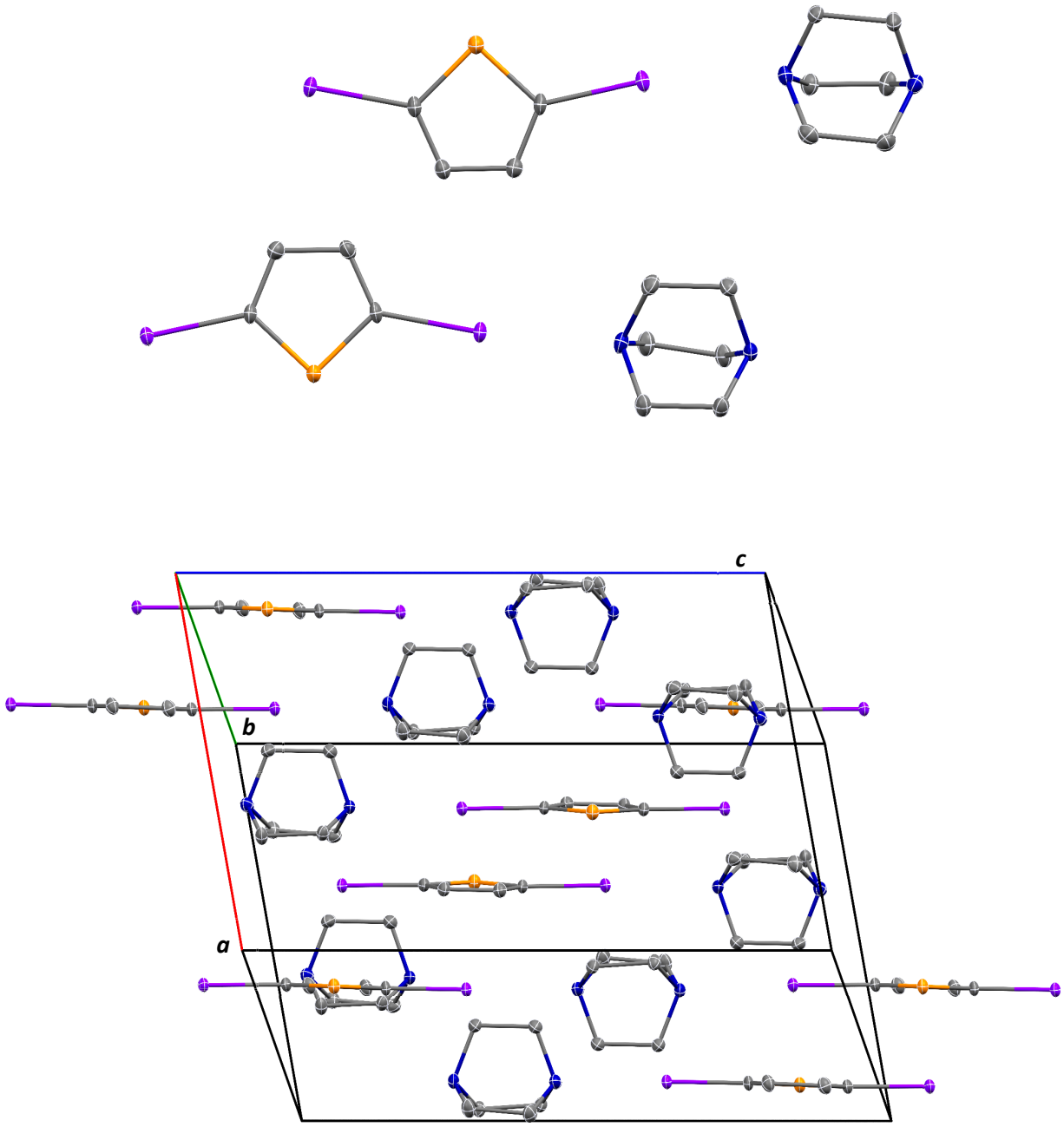

Figure SI3. Molecular structure (top) and unit cell packing (bottom) of (**25DIT**)·(**DABCO**). Hydrogen atoms are omitted for clarity. Atomic displacement ellipsoids are shown at the 50% probability level.

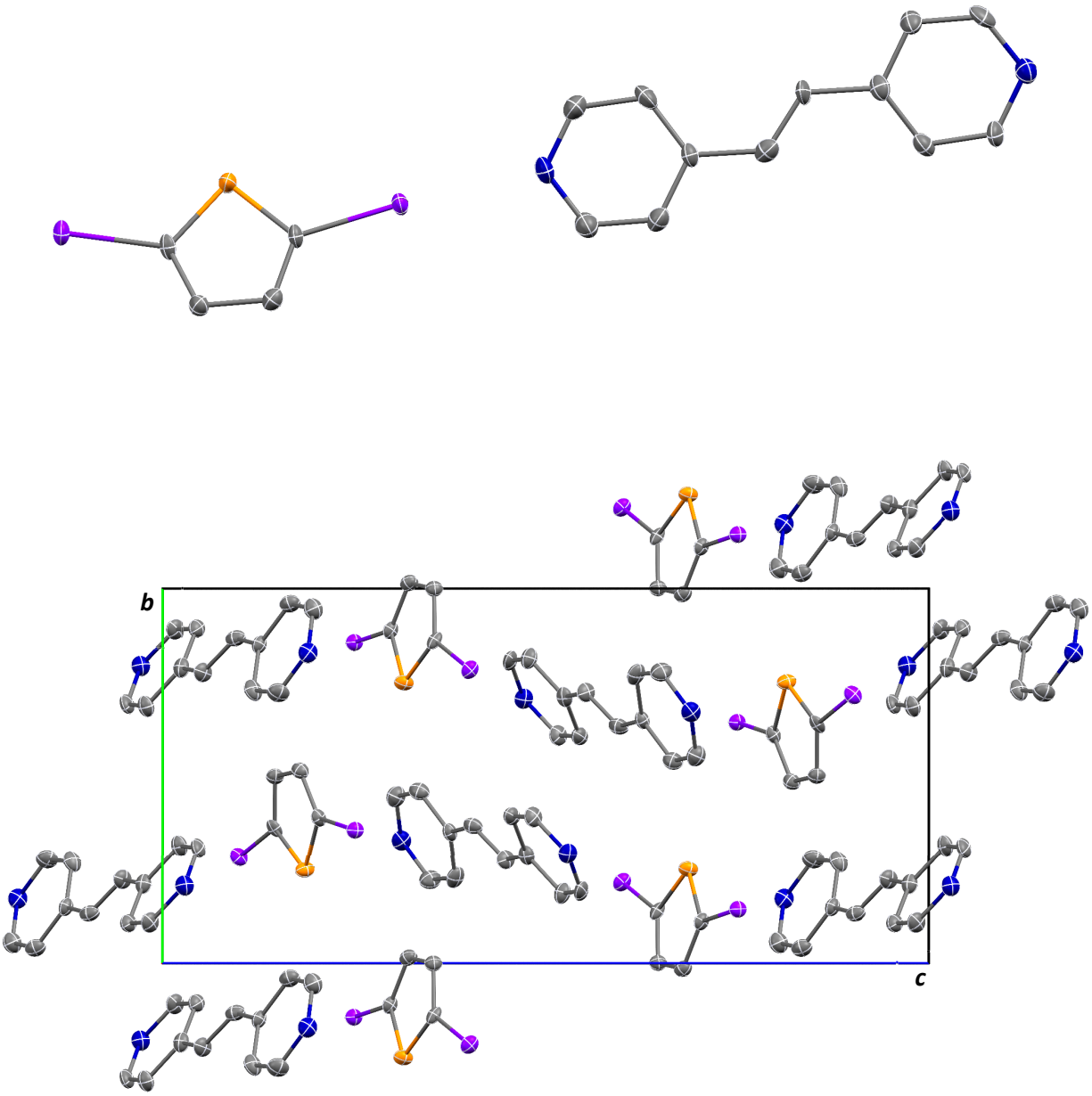

Figure SI4. Molecular structure (top) and unit cell packing (bottom) of (**25DIT**)·(**dpe**). Hydrogen atoms are omitted for clarity. Atomic displacement ellipsoids are shown at the 50% probability level.

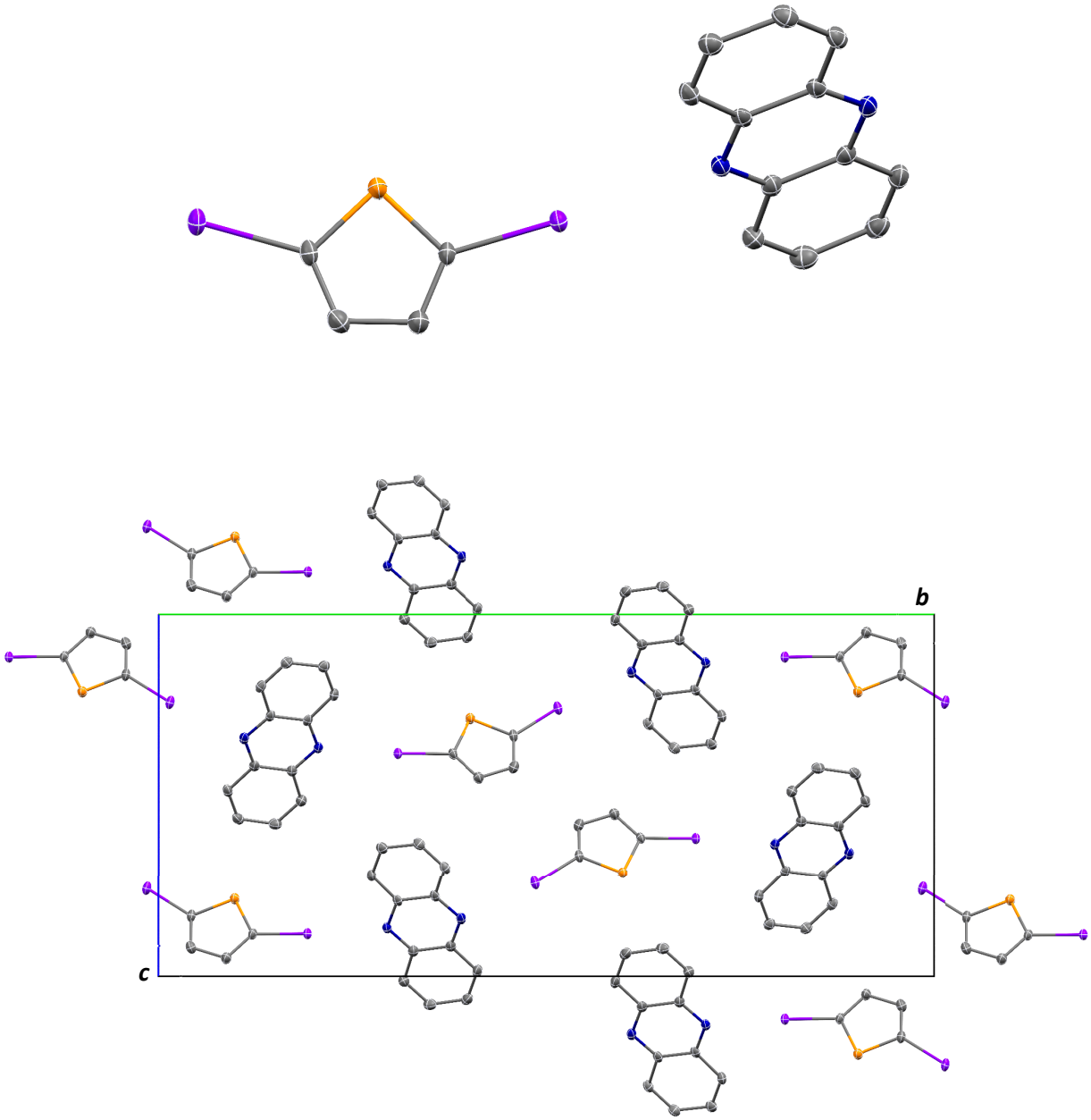

Figure SI5. Molecular structure (top) and unit cell packing (bottom) of (**25DIT**)·(**phenaz**). Hydrogen atoms are omitted for clarity. Atomic displacement ellipsoids are shown at the 50% probability level.

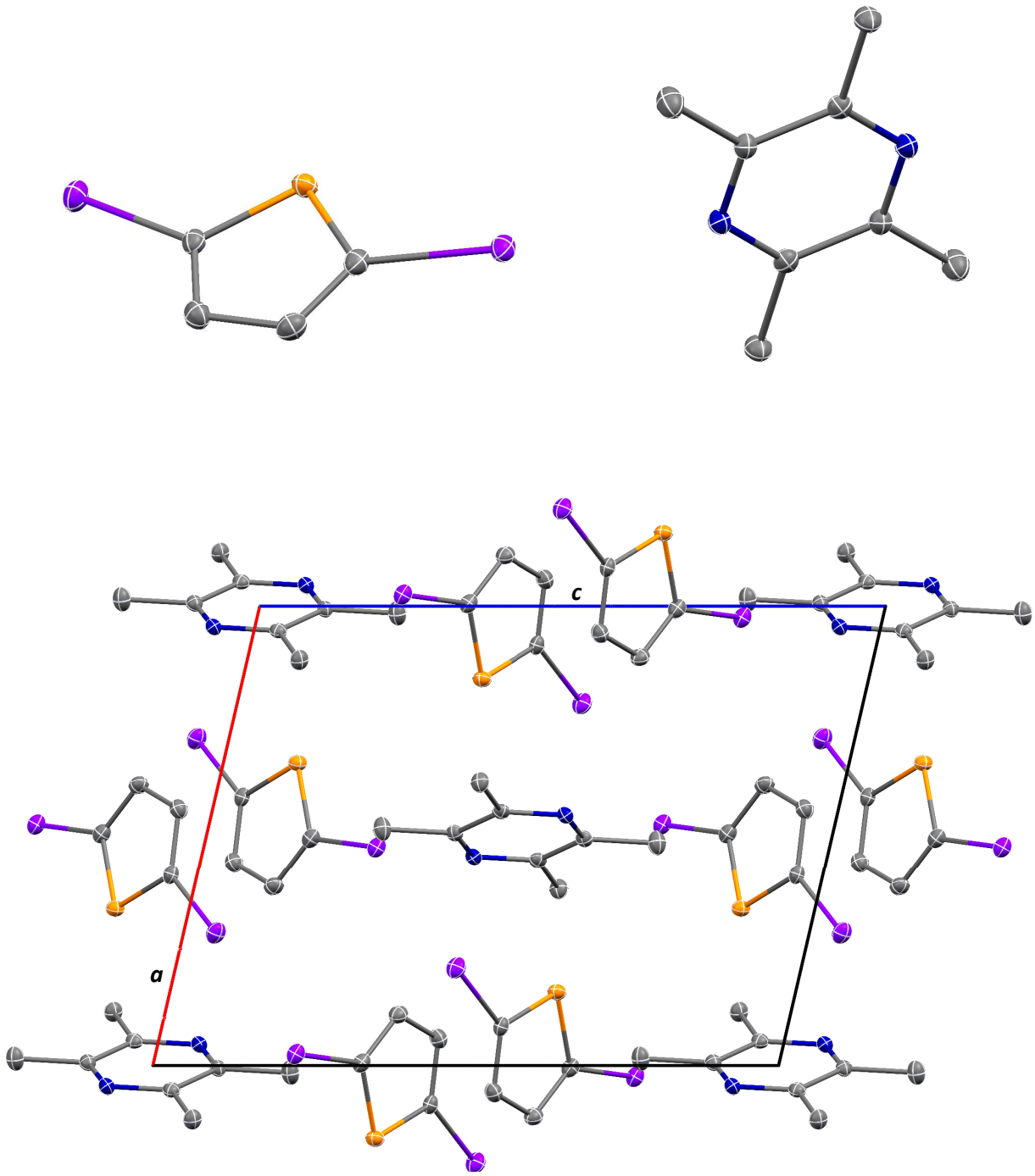

Figure SI6. Molecular structure (top) and unit cell packing (bottom) of 2(**25DIT**)·(**Me$_4$pyrz**). Hydrogen atoms are omitted for clarity. Atomic displacement ellipsoids are shown at the 50% probability level.

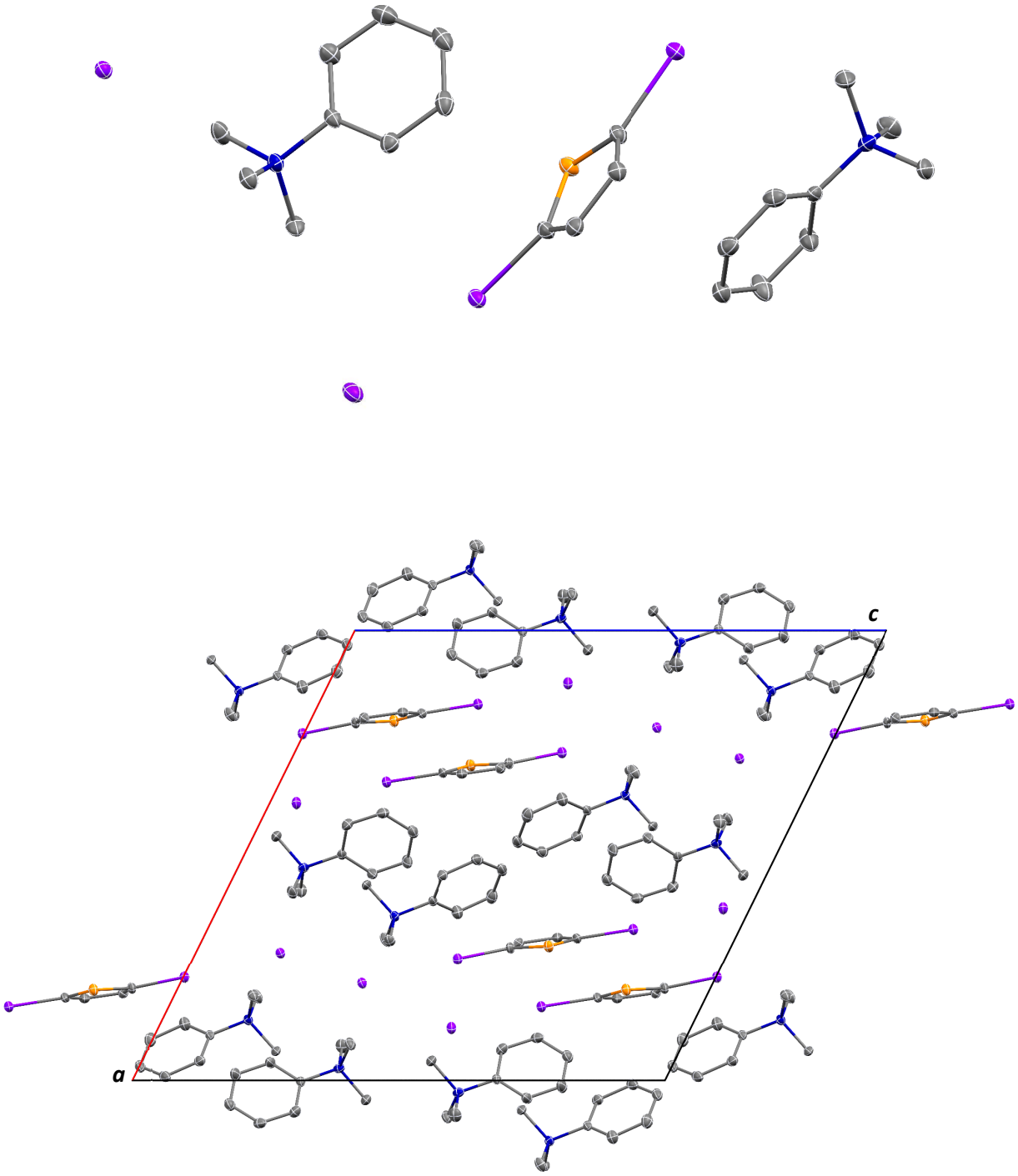

Figure SI7. Molecular structure (top) and unit cell packing (bottom) of (**25DIT**)·2(**NMe_3PhI**). Hydrogen atoms are omitted for clarity. Atomic displacement ellipsoids are shown at the 50% probability level.

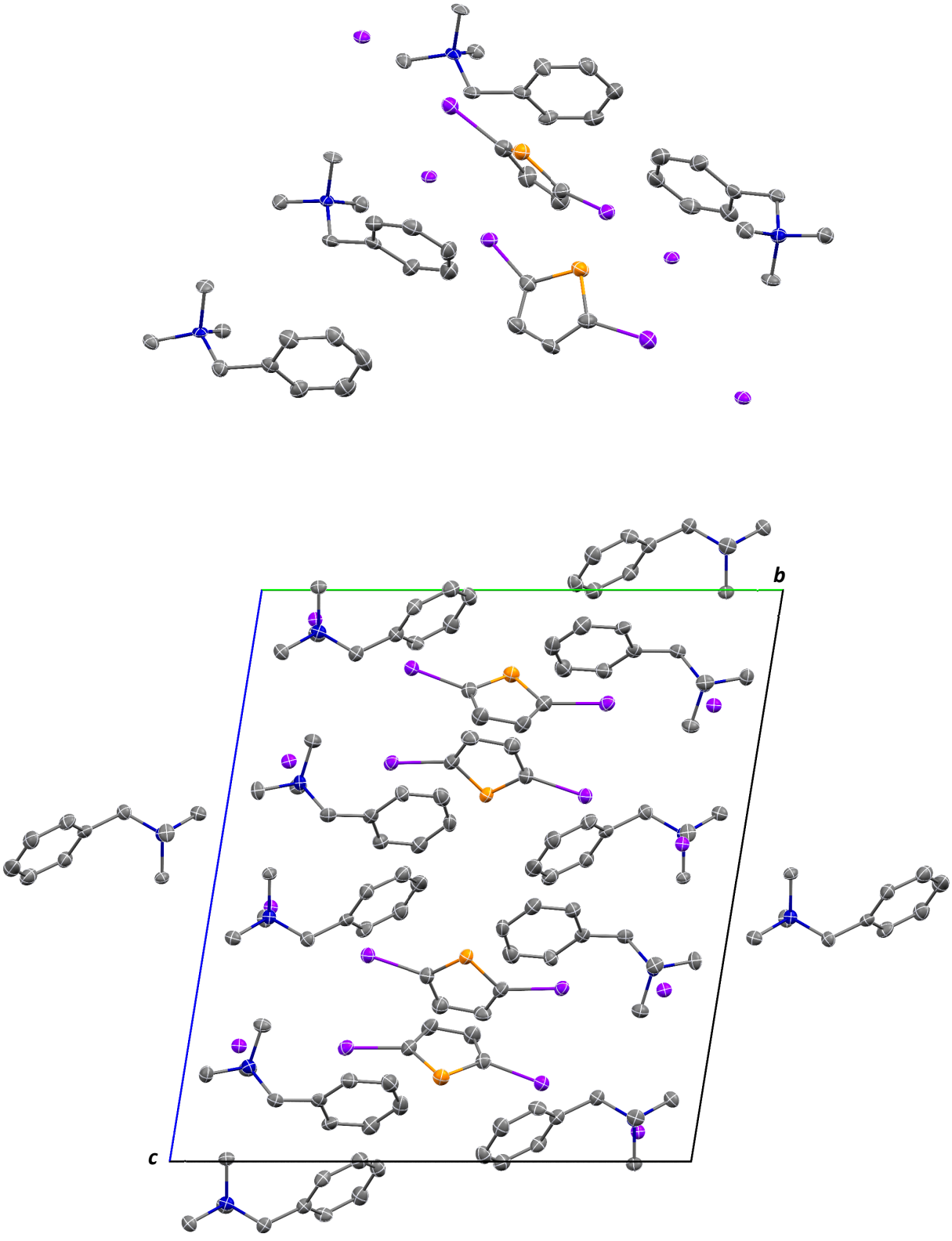

Figure SI8. Molecular structure (top) and unit cell packing (bottom) of (**25DIT**)·2(**NMe_3BzI**). Hydrogen atoms are omitted for clarity. Atomic displacement ellipsoids are shown at the 50% probability level.

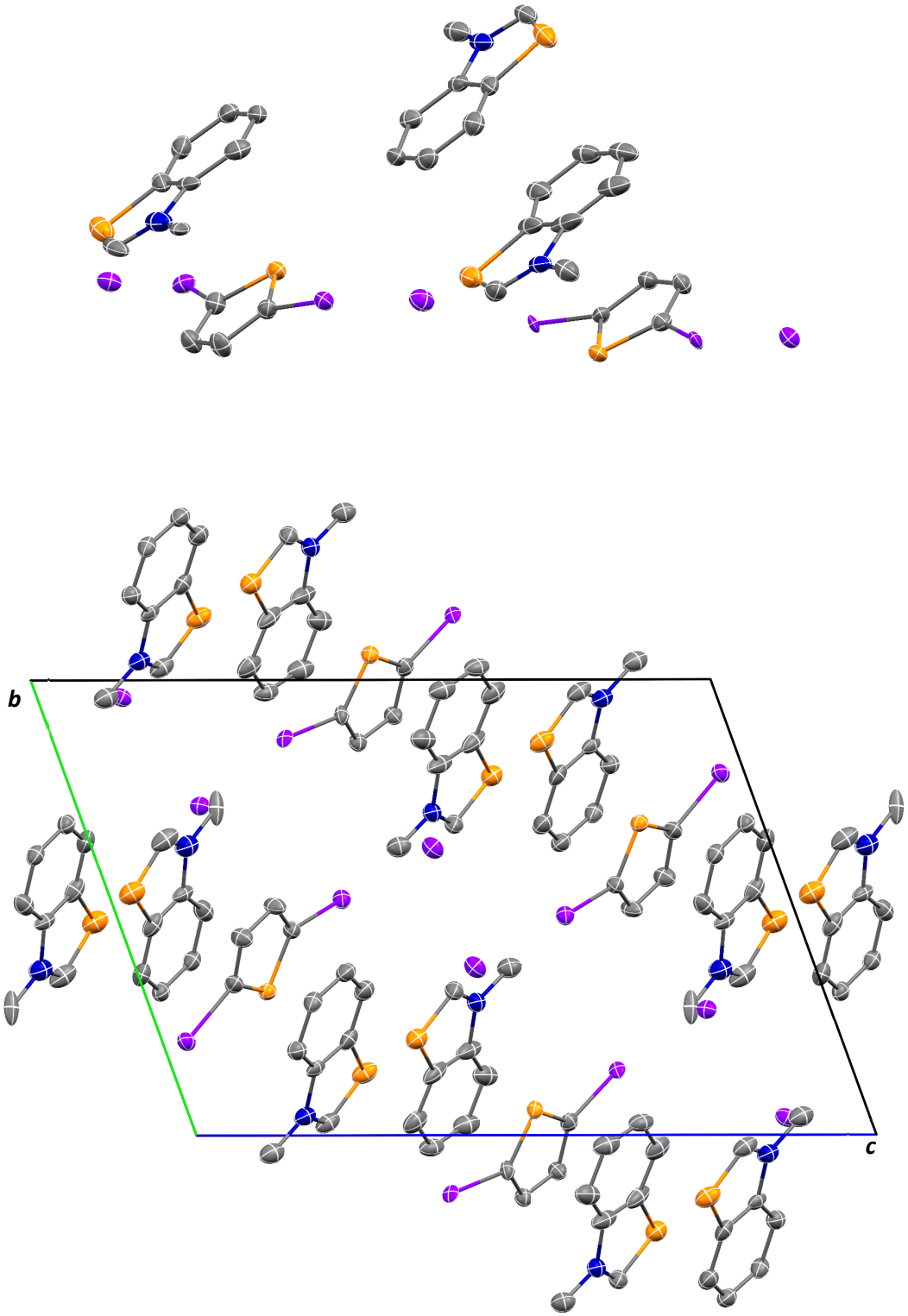

Figure SI9. Molecular structure (top) and unit cell packing (bottom) of (**25DIT**)·2(**NMeBenzoSI**). The atomic positions of one **25DIT** molecule are half-occupied, with the second half generated through inversion. Only the primary disorder component of **NMeBenzoSI** is shown. Hydrogen atoms are omitted for clarity. Atomic displacement ellipsoids are shown at the 50% probability level.

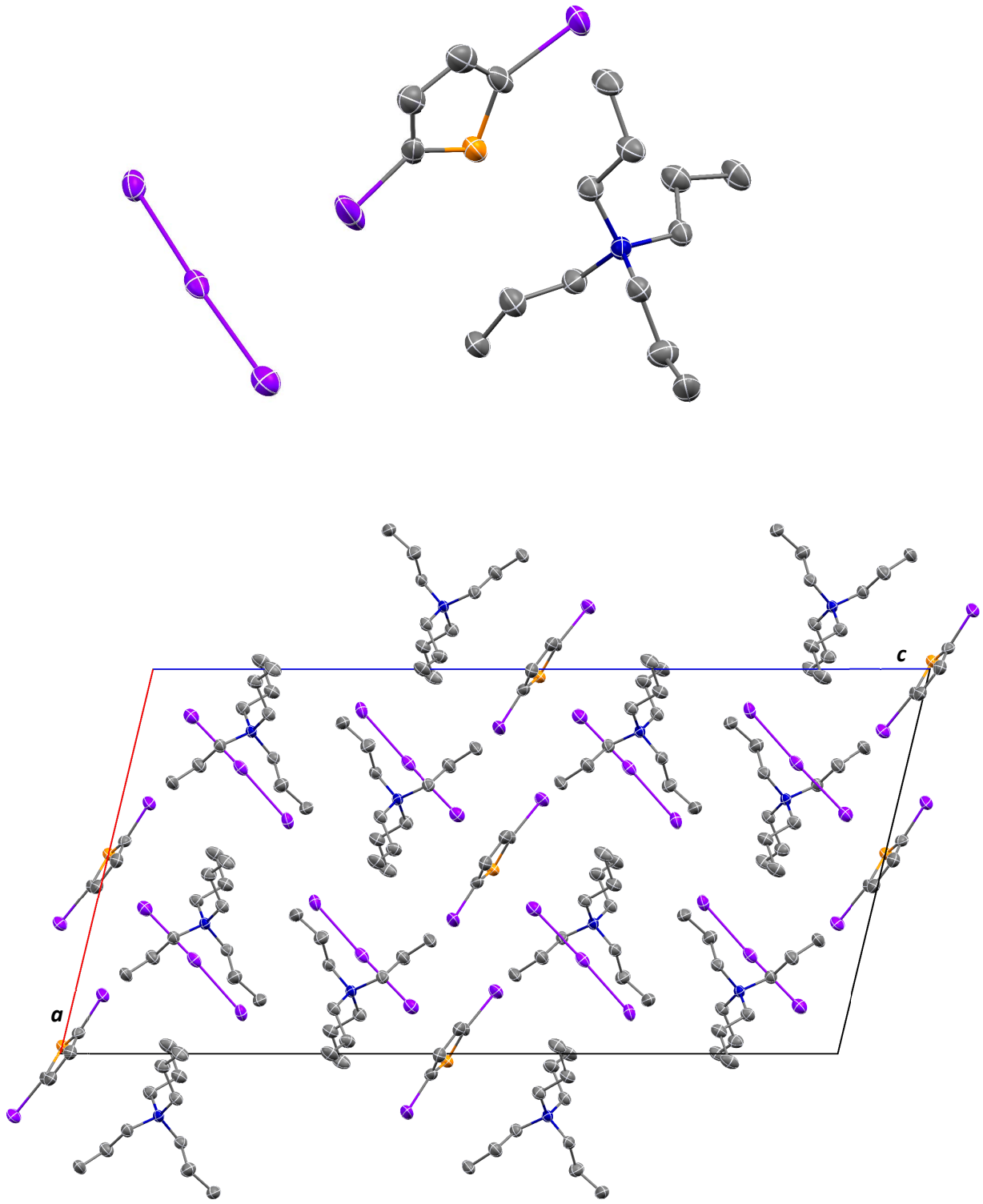

Figure SI10. Molecular structure (top) and unit cell packing (bottom) of (**25DIT**)·2(**NProp$_4$I$_3$**). The atomic positions of one **25DIT** molecule are half-occupied, with the second half generated through inversion. Only the primary disorder component of the triiodide anion is shown. Hydrogen atoms are omitted for clarity. Atomic displacement ellipsoids are shown at the 50% probability level.

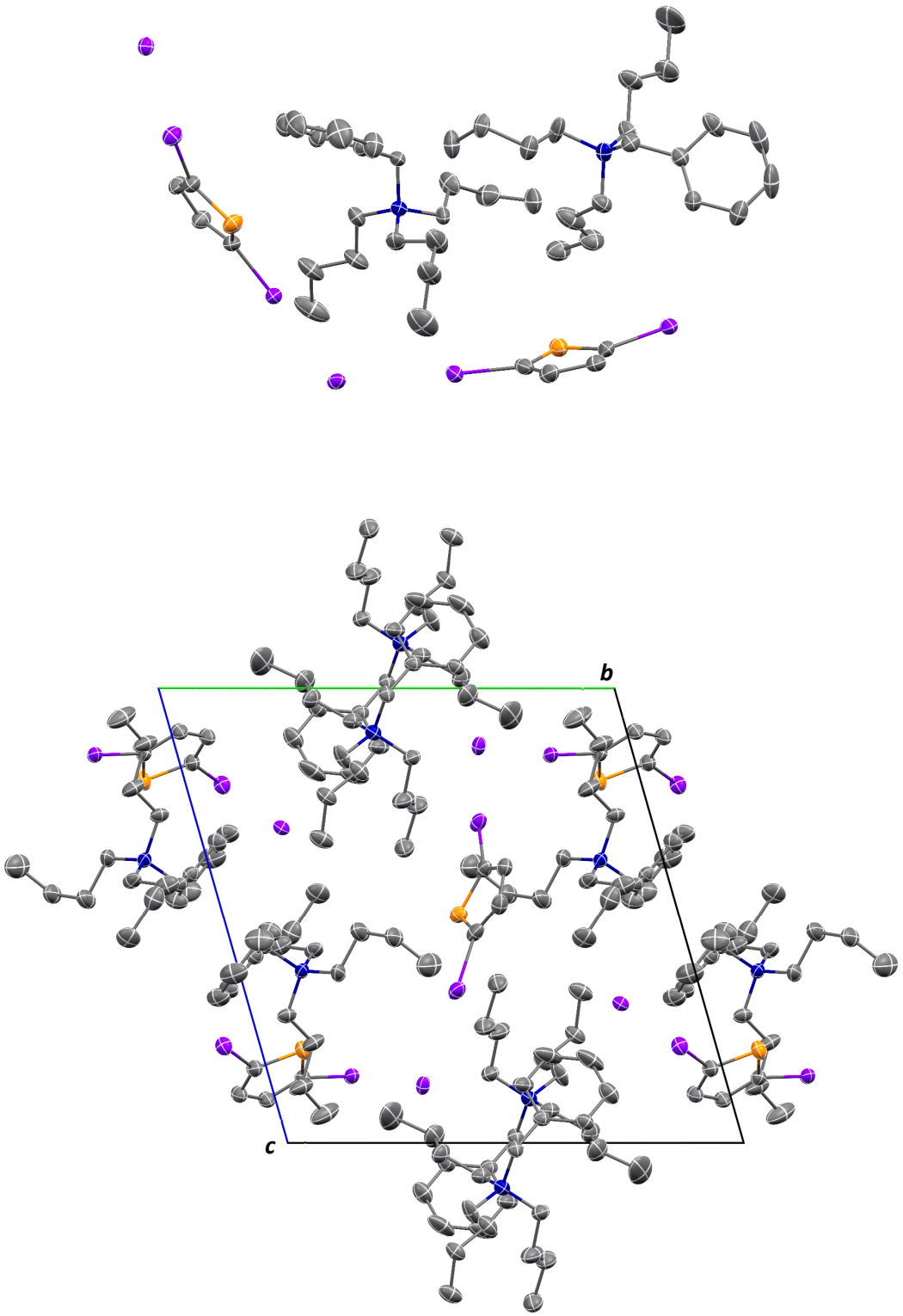

Figure SI11. Molecular structure (top) and unit cell packing (bottom) of 3(**25DIT**)·4(**NBut$_3$BzI**). The atomic positions of one **25DIT** molecule are half-occupied, with the second half generated through inversion. Only the primary disorder components of the butyl chains are shown. Hydrogen atoms are omitted for clarity. Atomic displacement ellipsoids are shown at the 50% probability level.

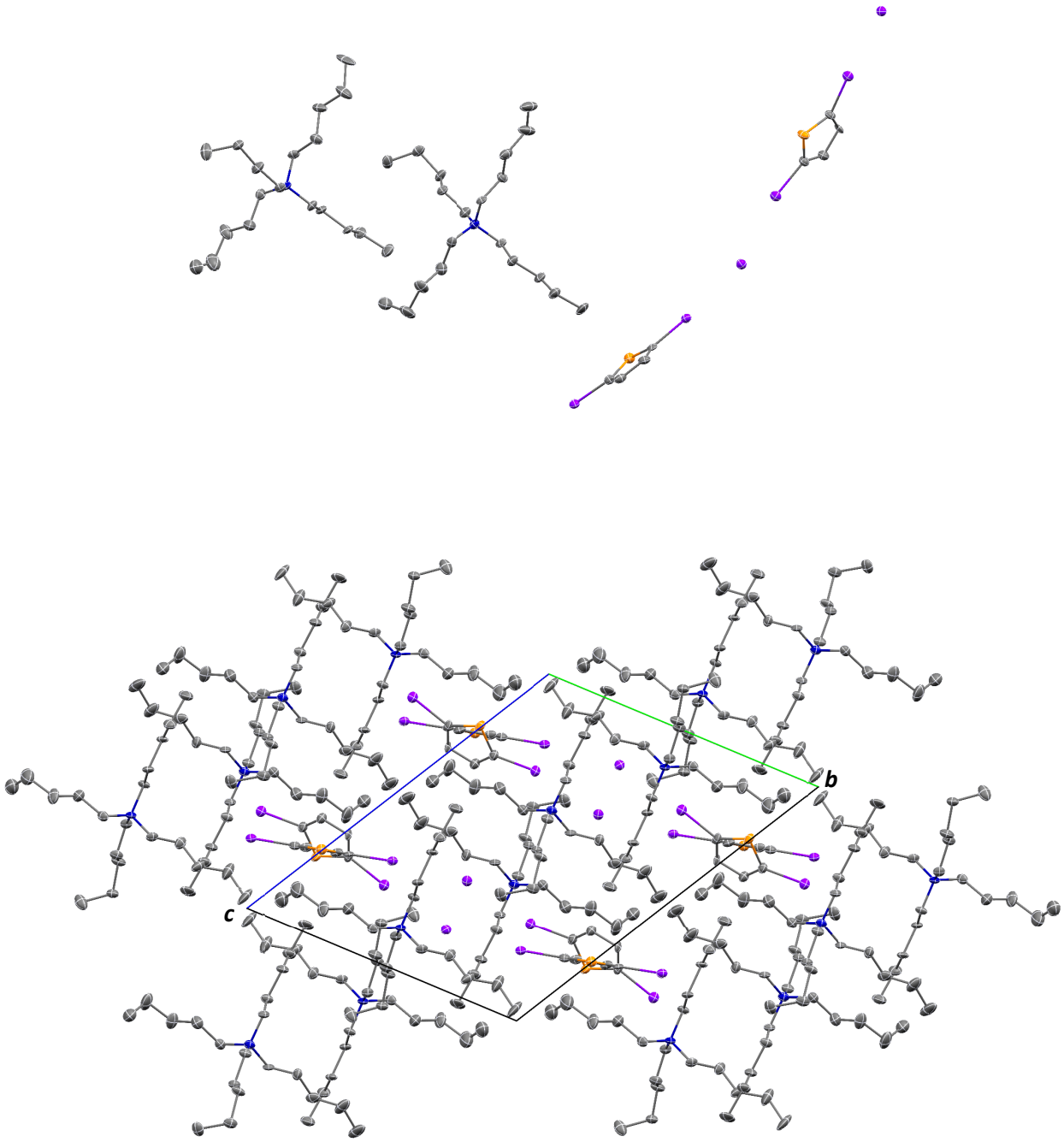

Figure SI12. Molecular structure (top) and unit cell packing (bottom) of (**25DIT**)·(**NPent$_4$I**). Only the primary disorder of the **25DIT** molecule is shown. Hydrogen atoms are omitted for clarity. Atomic displacement ellipsoids are shown at the 50% probability level.

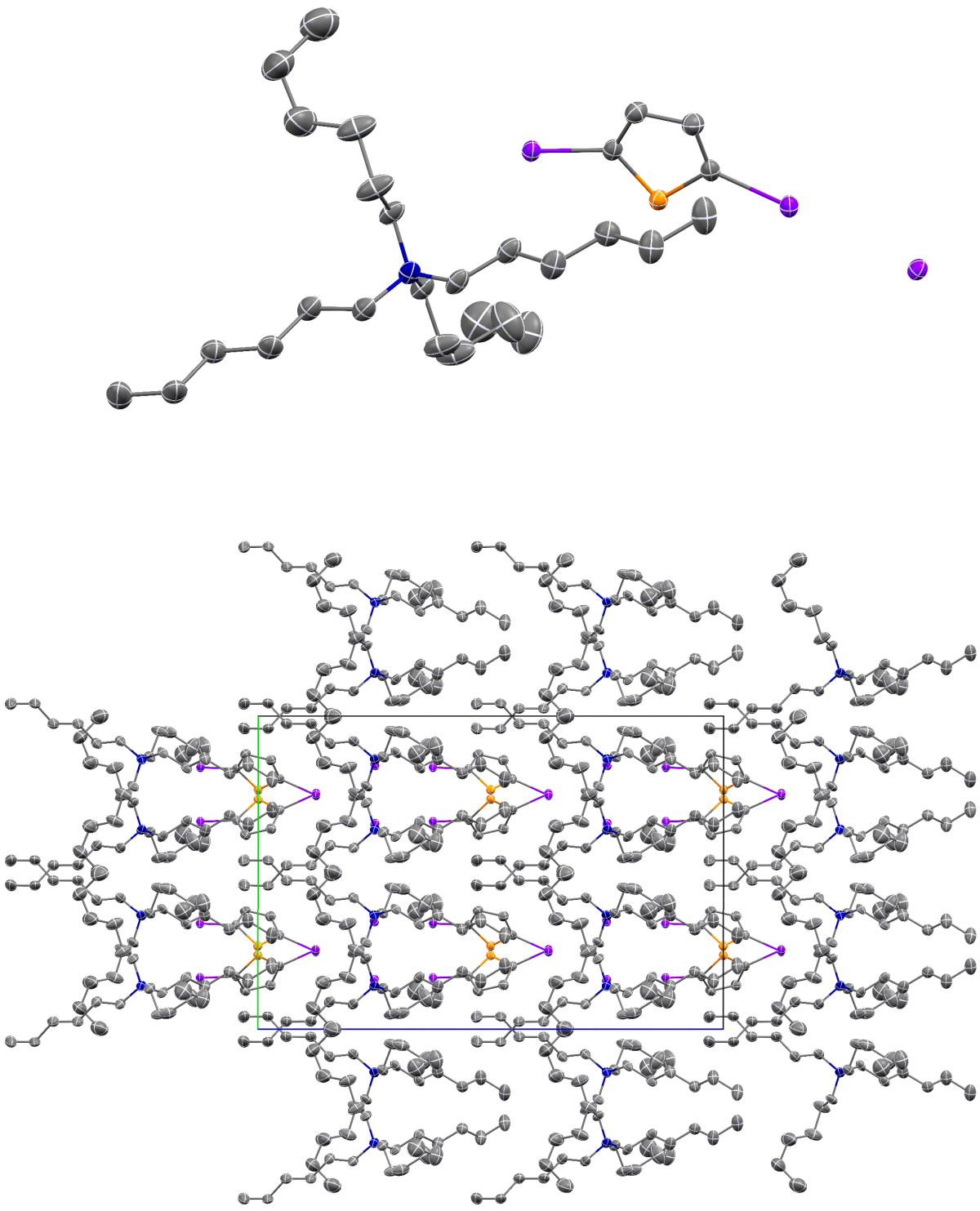

Figure SI13. Molecular structure (top) and unit cell packing (bottom) of (**25DIT**)·(**NHex$_4$I**). Hydrogen atoms are omitted for clarity. Atomic displacement ellipsoids are shown at the 50% probability level.

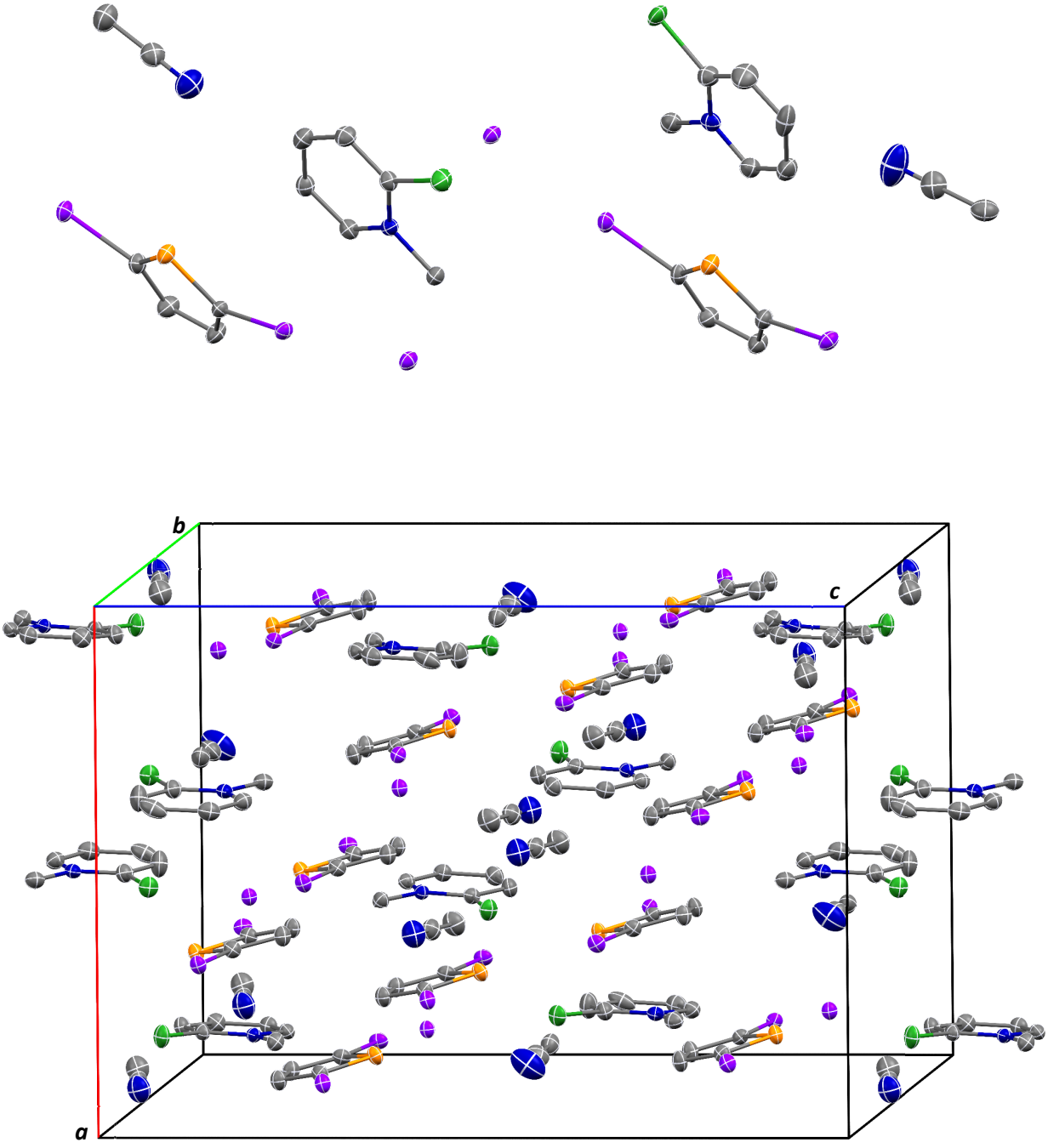

Figure SI14. Molecular structure (top) and unit cell packing (bottom) of (**25DIT**)·(**2Cl-NMePyrI**)·(**MeCN**). Hydrogen atoms are omitted for clarity. Atomic displacement ellipsoids are shown at the 50% probability level.

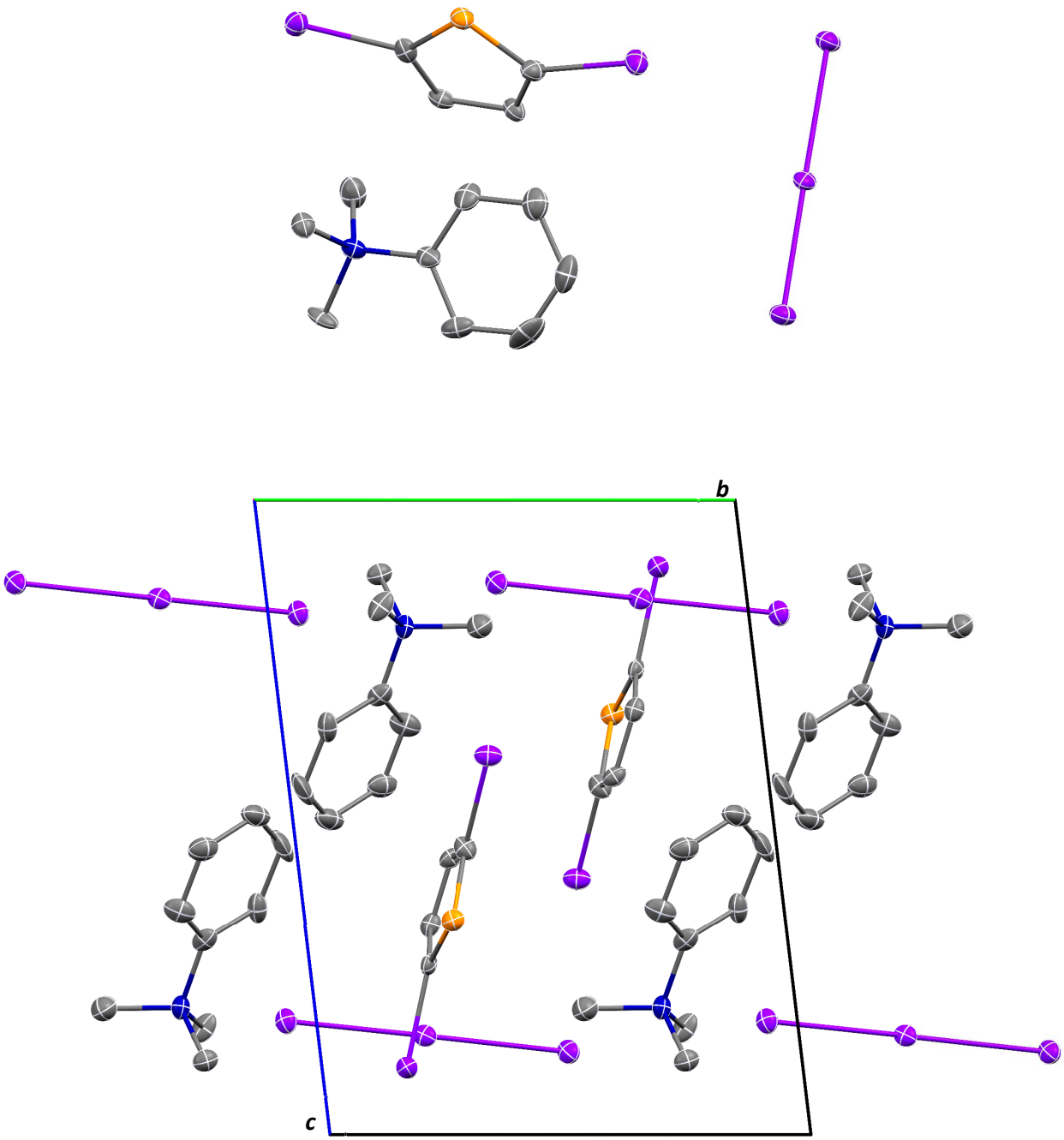

Figure SI15. Molecular structure (top) and unit cell packing (bottom) of (**25DIT**)·(**NMe_3PhI_3**). Hydrogen atoms are omitted for clarity. Atomic displacement ellipsoids are shown at the 50% probability level.

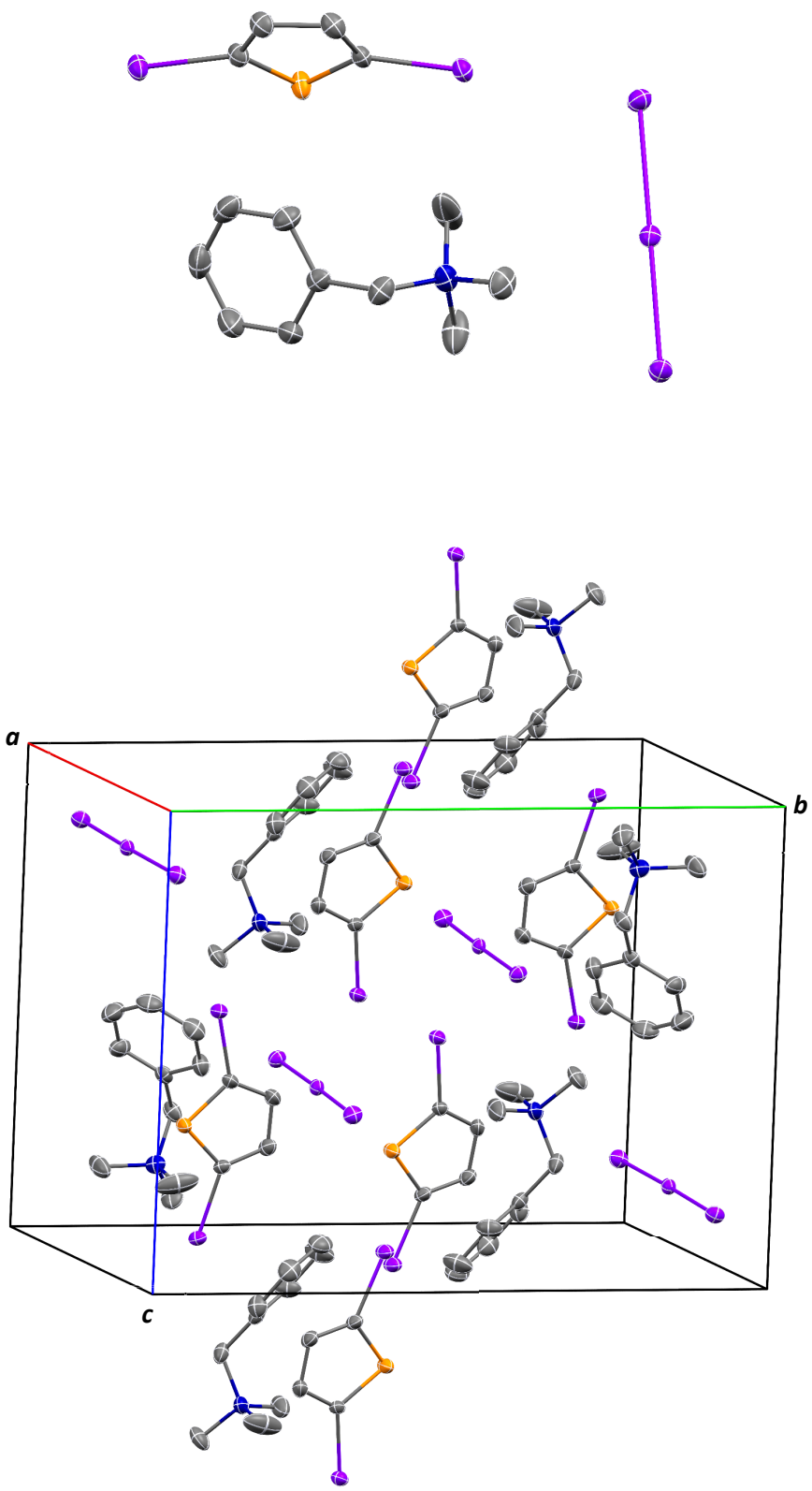

Figure SI16. Molecular structure (top) and unit cell packing (bottom) of (**25DIT**)·(**NMe_3BzI_3**). Hydrogen atoms are omitted for clarity. Atomic displacement ellipsoids are shown at the 50% probability level.

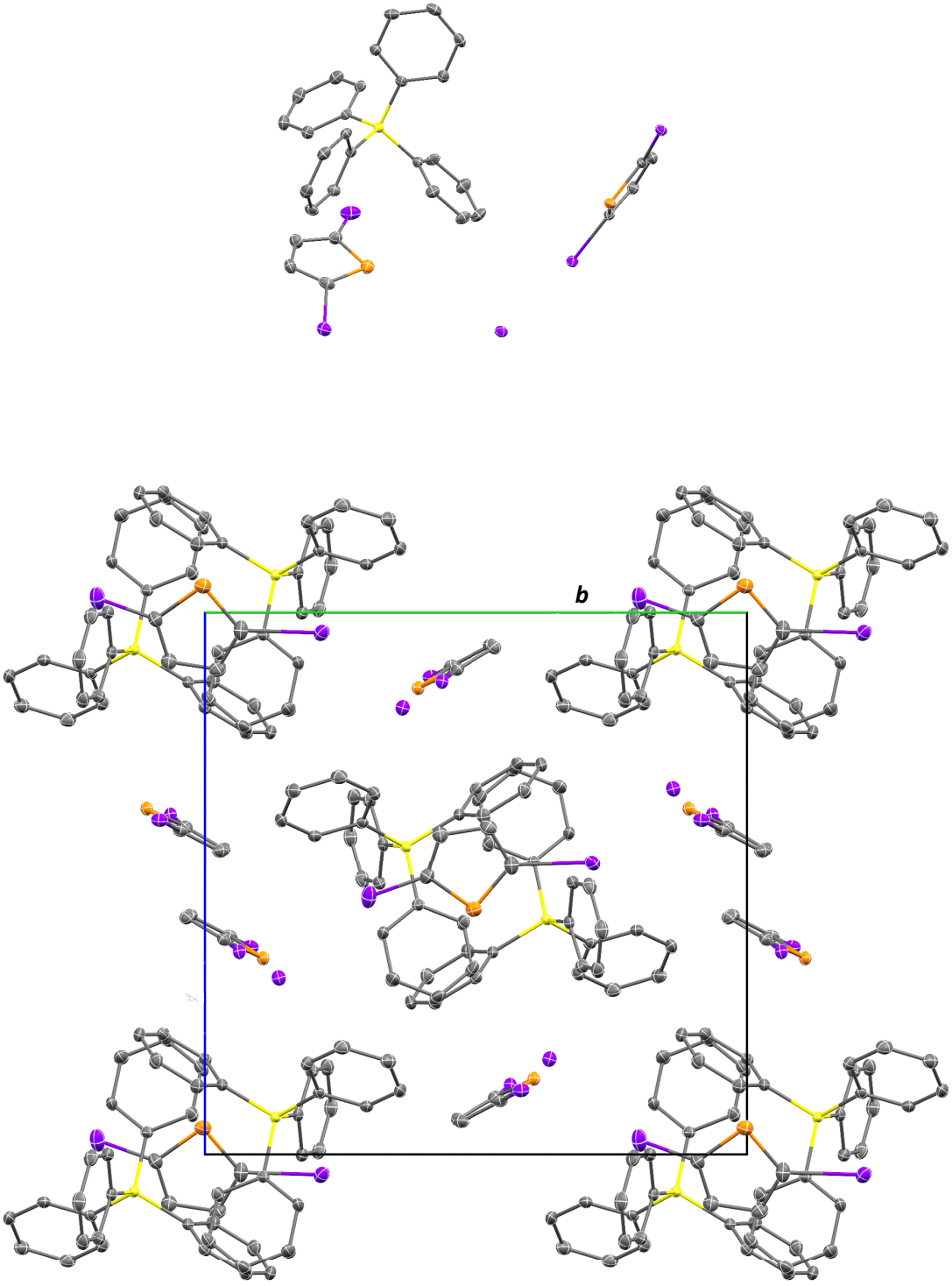

Figure SI17. Molecular structure (top) and unit cell packing (bottom) of 3(**25DIT**)·2(**PPh_4I**). The atomic positions of one **25DIT** molecule are half-occupied, with the second half generated through inversion. Hydrogen atoms are omitted for clarity. Atomic displacement ellipsoids are shown at the 50% probability level.

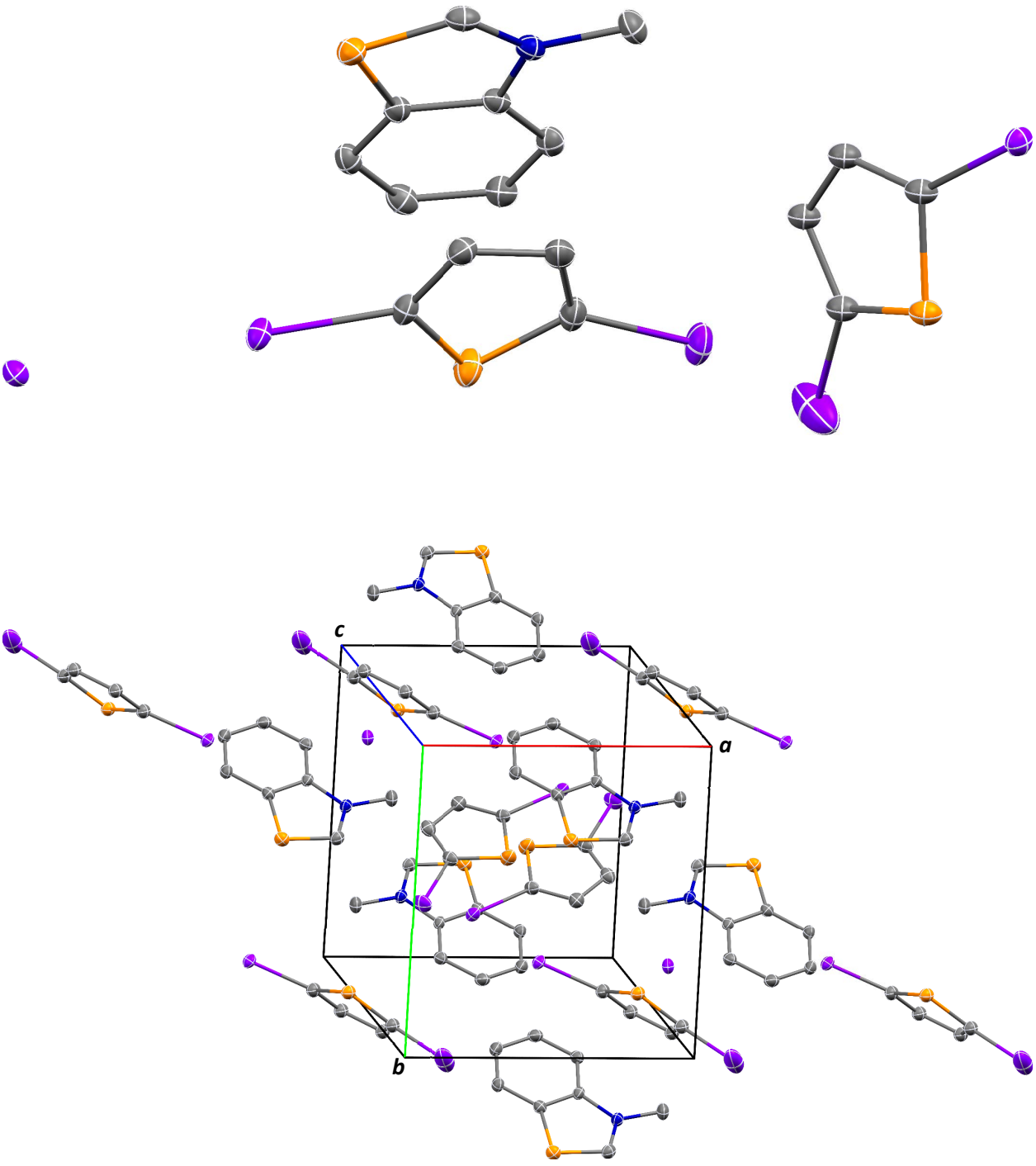

Figure SI18. Molecular structure (top) and unit cell packing (bottom) of 3(**25DIT**)·2(**NMeBenzoSI**). Only the primary disorder component is shown. Hydrogen atoms are omitted for clarity. Atomic displacement ellipsoids are shown at the 50% probability level.

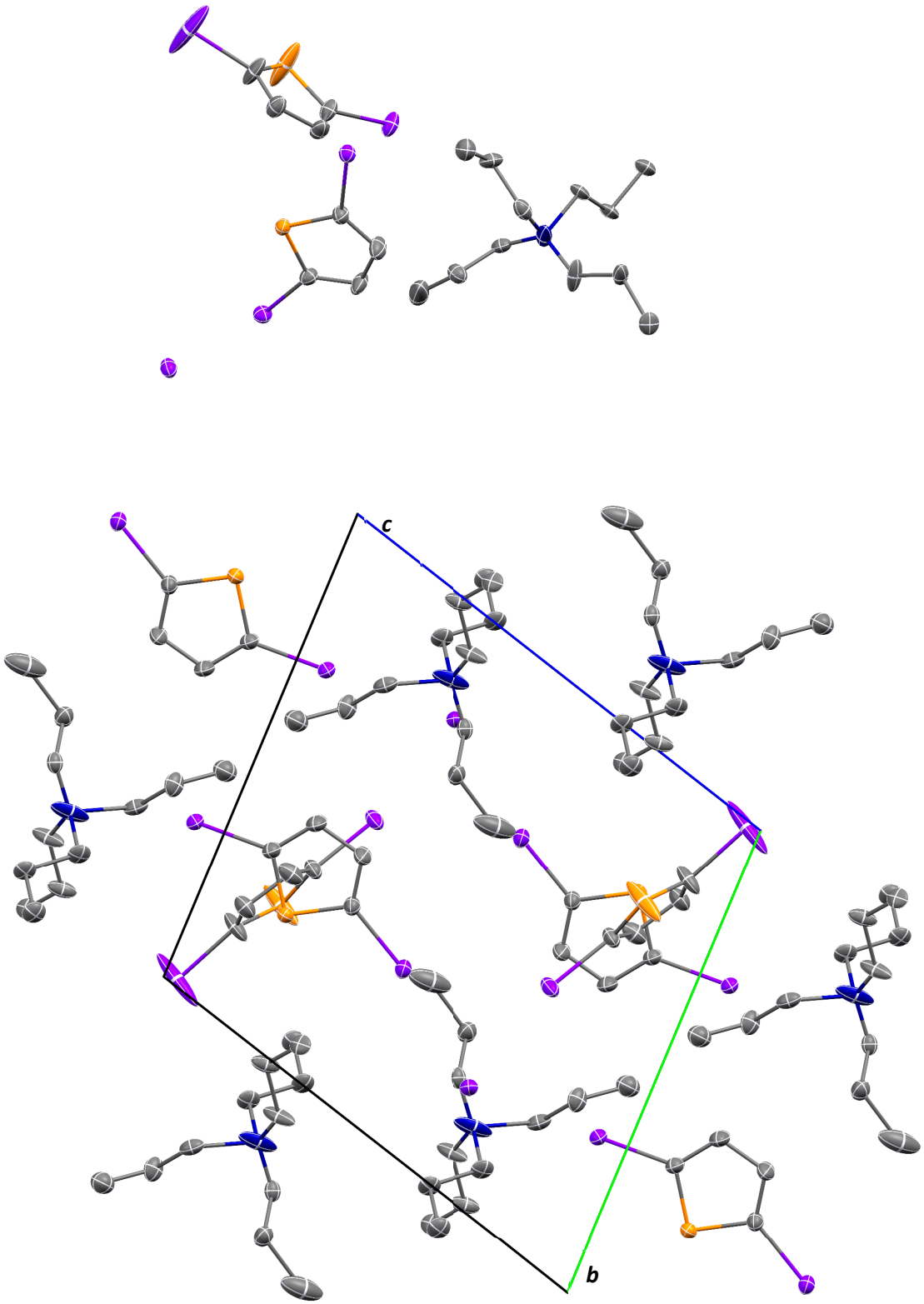

Figure SI19. Molecular structure (top) and unit cell packing (bottom) of 2(**25DIT**)·(**NProp$_4$I**). Only the primary disorder component of the propyl chains is shown. Hydrogen atoms are omitted for clarity. Atomic displacement ellipsoids are shown at the 50% probability level.

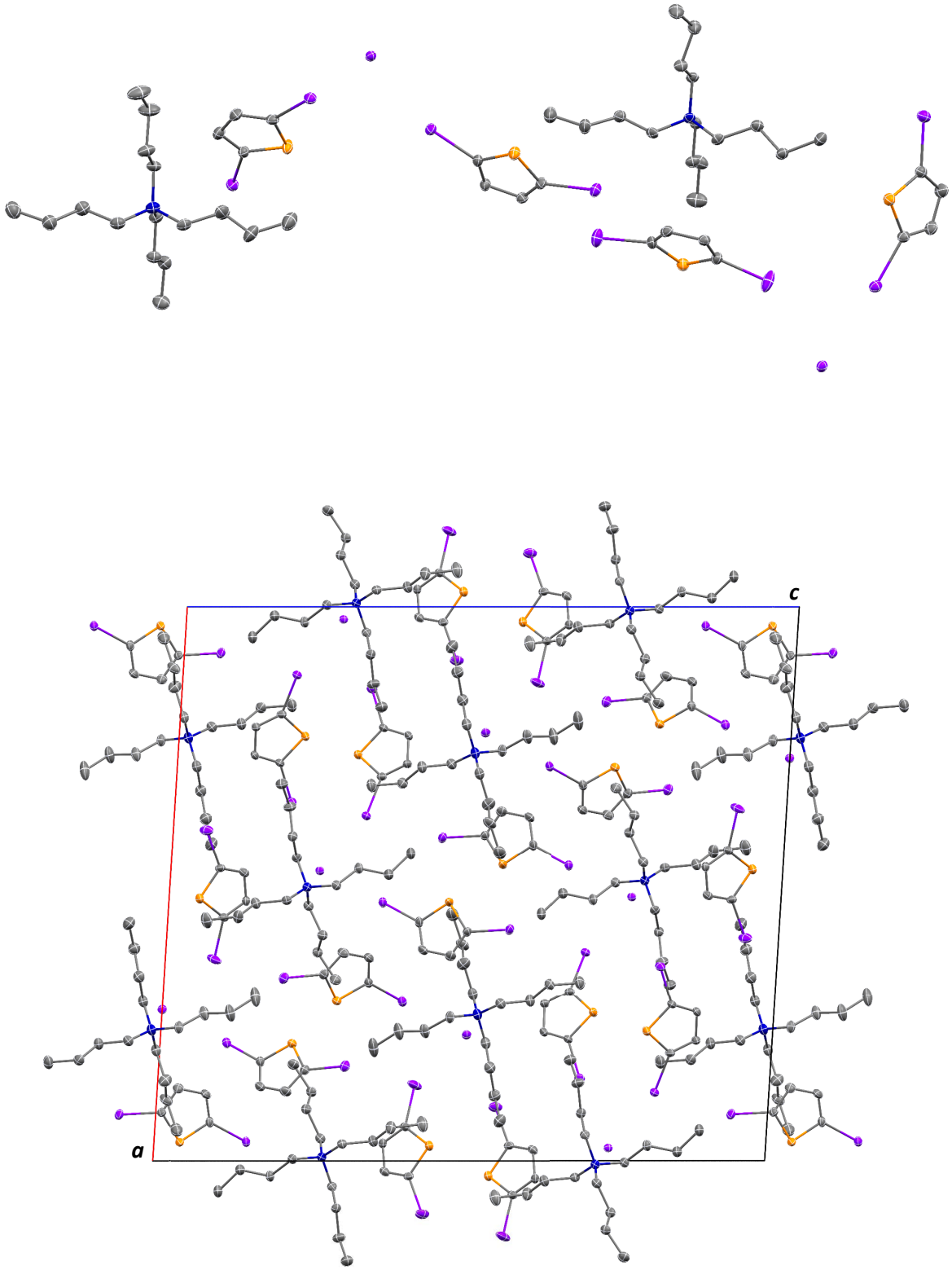

Figure SI20. Molecular structure (top) and unit cell packing (bottom) of 2(**25DIT**)·(**NBut$_4$I**). Hydrogen atoms are omitted for clarity. Atomic displacement ellipsoids are shown at the 50% probability level.